Research Paper

THEMED ISSUE: Geologic Evolution of the Alaska Range and Environs

GEOSPHERE

GEOSPHERE, v. 16

https://doi.org/10.1130/GES02127.1

18 figures; 3 tables; 1 set of supplemental files

CORRESPONDENCE: jtrop@bucknell.edu

CITATION: Trop, J.M., Benowitz, J.A., Koepp, D.Q., Sunderlin, D., Brueseke, M.E., Layer, P.W., and Fitzgerald, P.G., 2019, Stitch in the ditch: Nutzotin Mountains (Alaska) fluvial strata and a dike record ca. 117–114 Ma accretion of Wrangellia with western North America and initiation of the Totschunda fault: Geosphere, v. 16, https://doi.org/10.1130/GES02127.1.

Science Editor: Andrea Hampel
Guest Associate Editor: Graham D.M. Andrews

Received 17 February 2019
Revision received 6 August 2019
Accepted 9 October 2019

Stitch in the ditch: Nutzotin Mountains (Alaska) fluvial strata and a dike record ca. 117–114 Ma accretion of Wrangellia with western North America and initiation of the Totschunda fault

Jeffrey M. Trop[1], Jeffrey A. Benowitz[2], Donald Q. Koepp[1], David Sunderlin[3], Matthew E. Brueseke[4], Paul W. Layer[2], and Paul G. Fitzgerald[5]

[1]Department of Geology and Environmental Geosciences, Bucknell University, 701 Moore Avenue, Lewisburg, Pennsylvania 17837, USA
[2]Geophysical Institute and Geochronology Laboratory, University of Alaska–Fairbanks, Fairbanks, Alaska 99775, USA
[3]Department of Geology and Environmental Geosciences, Lafayette College, Easton, Pennsylvania 18042, USA
[4]Department of Geology, Kansas State University, Manhattan, Kansas 66506, USA
[5]Department of Earth Sciences, Syracuse University, Syracuse, New York 13244, USA

ABSTRACT

The Nutzotin basin of eastern Alaska consists of Upper Jurassic through Lower Cretaceous siliciclastic sedimentary and volcanic rocks that depositionally overlie the inboard margin of Wrangellia, an accreted oceanic plateau. We present igneous geochronologic data from volcanic rocks and detrital geochronologic and paleontological data from nonmarine sedimentary strata that provide constraints on the timing of deposition and sediment provenance. We also report geochronologic data from a dike injected into the Totschunda fault zone, which provides constraints on the timing of intra–suture zone basinal deformation. The Beaver Lake formation is an important sedimentary succession in the northwestern Cordillera because it provides an exceptionally rare stratigraphic record of the transition from marine to nonmarine depositional conditions along the inboard margin of the Insular terranes during mid-Cretaceous time. Conglomerate, volcanic-lithic sandstone, and carbonaceous mudstone/shale accumulated in fluvial channel-bar complexes and vegetated overbank areas, as evidenced by lithofacies data, the terrestrial nature of recovered kerogen and palynomorph assemblages, and terrestrial macrofossil remains of ferns and conifers. Sediment was eroded mainly from proximal sources of upper Jurassic to lower Cretaceous igneous rocks, given the dominance of detrital zircon and amphibole grains of that age, plus conglomerate with chiefly volcanic and plutonic clasts. Deposition was occurring by ca. 117 Ma and ceased by ca. 98 Ma, judging from palynomorphs, the youngest detrital ages, and ages of crosscutting intrusions and underlying lavas of the Chisana Formation. Following deposition, the basin fill was deformed, partly eroded, and displaced laterally by dextral displacement along the Totschunda fault, which bisects the Nutzotin basin. The Totschunda fault initiated by ca. 114 Ma, as constrained by the injection of an alkali feldspar syenite dike into the Totschunda fault zone.

These results support previous interpretations that upper Jurassic to lower Cretaceous strata in the Nutzotin basin accumulated along the inboard margin of Wrangellia in a marine basin that was deformed during mid-Cretaceous time. The shift to terrestrial sedimentation overlapped with crustal-scale intrabasinal deformation of Wrangellia, based on previous studies along the Lost Creek fault and our new data from the Totschunda fault. Together, the geologic evidence for shortening and terrestrial deposition is interpreted to reflect accretion/suturing of the Insular terranes against inboard terranes. Our results also constrain the age of previously reported dinosaur footprints to ca. 117 Ma to ca. 98 Ma, which represent the only dinosaur fossils reported from eastern Alaska.

INTRODUCTION

Suturing of fragments of continental crust, island arcs, and overthickened oceanic crust following the subduction of intervening oceanic lithosphere is a fundamental process in plate dynamics and the growth of Earth's continents. The suturing process itself results in changes in plate dynamics, creates Earth's largest mountain belts, and changes global climate dynamics by closing ocean basins and forming high topography (e.g., Coney et al., 1980; Raymo et al., 1988; Zhu et al., 2005; Najman et al., 2010). Although a fundamental and global tectonic process, details of this process remain poorly understood. Well-exposed geologic records of past suturing events await detailed investigation using modern analytical techniques (e.g., Finzel et al., 2011; Benowitz et al., 2014, 2019; Orme et al., 2015). Ancient suture zones crop out across Earth's continents in regional structural, sedimentary, and petrologic trends that extend hundreds to thousands of kilometers along strike. Such zones of deformation are rarely characterized by simple, single, easily recognizable lines but instead may be zones of deformation hundreds of kilometers wide (Dewey, 1977). Suture zones are syncollisional features but often also serve as postcollisional zones of crustal weakness prone to reactivation (Dewey, 1977; Hendrix et al., 1996; Holdsworth et al., 2001; Cavazza et al., 2017; Laskowski et al., 2017; Trop et al., 2019). These high-strain zones are often reactivated as strike-slip faults that laterally shuffle the upper plate (e.g., the Denali fault system; Fitzgerald et al., 2014). The timing of fault initiation can provide independent controls on the timing of accretion (Duvall et al., 2011). Geologic records preserved within suture zones provide an archive

of the evolution of tectonic processes during and following welding of crustal fragments, including deformation, magmatism, and sedimentation.

The northern Cordillera of western North America is an archetypal example of continental growth through accretionary tectonic processes. It is a complex collage of allochthonous terranes, sedimentary basins, magmatic belts, and subduction complex strata accreted to the continental margin, especially during Mesozoic to recent time (Coney et al., 1980; Plafker and Berg, 1994; Trop and Ridgway, 2007; Colpron et al., 2007; Gehrels et al., 2009). The Alexander, Wrangellia, and Peninsular terranes amalgamated during Paleozoic time, collided with the continental margin, and shuffled laterally along strike-slip faults, including the Denali, Totschunda, and Duke River faults (Fig. 1; Plafker and Berg, 1994; Cowan et al., 1997; Stamatakos et al., 2001; Roeske et al., 2003; Gabrielse et al., 2006; Wyld et al., 2006; Bacon et al., 2012). The Alexander terrane and Wrangellia, together with the Peninsular terrane, are collectively referred to as the Insular composite terrane (Colpron et al., 2007), or the Wrangellia composite terrane (Plafker and Berg, 1994).

The precise location of initial collision of the Insular terranes with the former continental margin is controversial (Cowan et al., 1997; Stamatakos et al., 2001), and the timing of initial collision may have been diachronous (Trop and Ridgway, 2007). Geologic evidence from southeastern Alaska and coastal British Columbia indicates mid-Jurassic accretion (e.g., McClelland and Gehrels, 1990; McClelland et al., 1992; van der Heyden, 1992; Monger et al., 1994; Monger, 2014), whereas data sets reported from south-central Alaska indicate Late Jurassic–Early Cretaceous accretion (e.g., Plafker and Berg, 1994; Trop and Ridgway, 2007; Hampton et al., 2017; Stevens Goddard et al., 2018). Thus, accretion may have been diachronous from south to north (e.g., Trop and Ridgway, 2007).

In south-central Alaska, the Insular terranes are juxtaposed against inboard terranes along a broad zone of deformation that spans a region as much as 100 km wide in the eastern and central Alaska Range and northern Talkeetna Mountains (Fig. 1; Csejtey et al., 1992; Nokleberg et al., 1992; Ridgway et al., 2002). This zone of deformation has

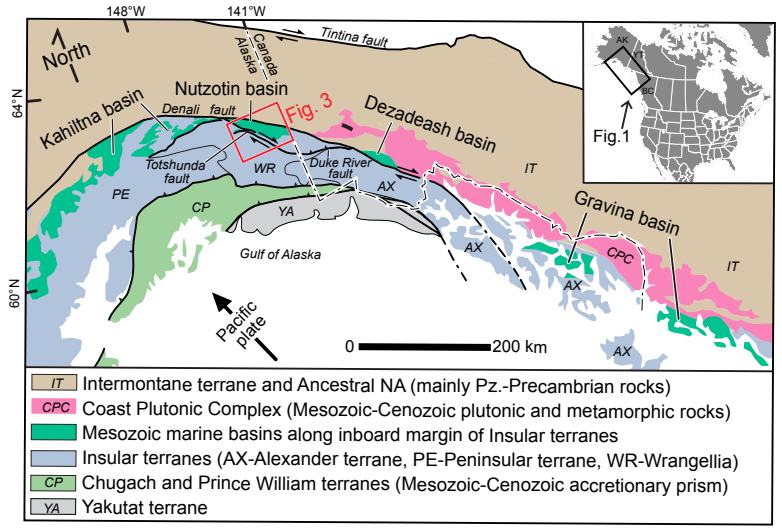

Figure 1. Map showing major terranes and faults along the northern North American Cordillera margin. Marine sedimentary basin deposits (dark green) record accretion of the Insular terranes (Alexander, Wrangellia, and Peninsular terranes—gray) against older inboard Intermontane terranes (brown). This study focuses the Nutzotin basin. Red rectangles mark focus areas shown in Figure 3. Figure is modified from Wilson et al. (2015). Inset map shows location of Figure 1 in North America (NA). Abbreviations: AK—Alaska, USA; BC—British Columbia, Canada; YT—Yukon Territory, Canada; Pz—Paleozoic.

been referred to as the Alaska Range suture zone (Ridgway et al., 2002; Brennan et al., 2011) or mega–suture zone (Jones et al., 1982). Geophysical data sets indicate that the suture zone is a crustal-scale feature between the Hines Creek fault on the north and the Talkeetna fault on the south (Brennan et al., 2011; Fitzgerald et al., 2014), although deformation extends outside the region between these major faults (Ridgway et al., 2002). Originally identified from rock types and deformation patterns at the surface (Jones et al., 1982; Ridgway et al., 2002), geophysical studies demonstrate that the suture zone proper extends through the crust. The Hines Creek and Talkeetna faults appear to continue through the crust nearly vertically and extend into the mantle (Brennan et al., 2011); seismic velocities differ substantially across the Denali and Totschunda faults (Allam et al., 2017). In eastern Alaska, the suture zone is not as well understood, owing to fewer geologic and geophysical data sets. However, a zone of deformation spans a region as much as 100 km wide in the eastern Alaska Range, Nutzotin Mountains, and Wrangell Mountains (Richter, 1976; Trop et al., 2002; Manuszak et al., 2007). Geophysical data sets indicate that the suture zone is a crustal-scale feature between the Denali fault on the north and the Totschunda fault on the south (Fig. 1; Allam et al., 2017), although deformation extends outside the region between these major faults (Trop et al., 2002; Manuszak et al., 2007). In southeastern Alaska, the zone is characterized by known and inferred, mid-Cretaceous inboard-dipping (east-dipping) thrust faults and intrusions that deform marine sedimentary strata of the Gravina basin (Crawford et al., 1987; Rubin and Saleeby, 1991; Gehrels et al., 1992).

Precise age constraints of sedimentary strata along the entire suture zone are critical to understanding the geodynamic drivers of basin development and may shed light on along-strike variations in suture zone evolution. The suture zone between colliding terranes typically transitions

from marine to terrestrial deposition in response to crustal shortening and uplift during accretion. The precise timing of subaerial emergence of the suture zone preserved in Alaska is not well constrained, owing partly to the paucity of terrestrial sedimentary strata preserved in depositional contact above the marine strata. Along the >3000-km-long suture zone, Jurassic–Cretaceous marine strata are depositionally overlain by nonmarine strata at only two known localities. Hampton et al. (2010, 2017) documented Albian–Cenomanian fluvial strata in a <100 km^2 outcrop belt in the northern Talkeetna Mountains. Richter (1976) reported isolated outcrops of "continental sedimentary rocks" in a handful of outcrops in the Nutzotin Mountains. These unnamed strata provide a unique opportunity for documenting the timing and nature of subaerial emergence of the suture zone during accretion of Wrangellia.

The terrestrial strata are truncated by the Totschunda fault, a lithospheric-scale structure that bisects the suture zone (Fig. 1; Allam et al., 2017). Given that lithospheric strength contrasts in suture zones are often reactivated as long-lived structures (Fitzgerald et al., 2014), constraining the long-term history of lithospheric-scale faults can provide additional constraints on the suturing process. Various possible inception ages for the Totschunda fault have been previously proposed: early Cenozoic and possibly earlier (Goldfarb et al., 2013), Oligocene (Brueseke et al., 2019), middle Miocene (Trop et al., 2012), and middle Pleistocene (Richter and Matson, 1971; Plafker et al., 1977). The fault may have an even longer history of deformation, given that seismic velocities differ substantially across the fault (Allam et al., 2017), and it may provide insight in the deformation history of the Insular terrane during accretion. However, geochronologic data from the fault zone are sparse.

In this study, we present the results of field mapping and sedimentologic, stratigraphic, and geochronologic analysis of terrestrial strata that record subaerial emergence and deformation of the formerly marine Late Jurassic–Early Cretaceous Nutzotin basin along the inboard margin of Wrangellia. Sedimentologic and paleontological data were combined to document the transition of depositional environments from marine to terrestrial conditions. Igneous and detrital geochronology and palynology were used to quantify the timing of sedimentation and deformation. Detrital ages were compared with previously reported ages from adjacent terranes to reconstruct sediment provenance. Additional constraints on accretion were provided by dating a dike that crosscuts fault gouge in the Totschunda fault zone, which truncates the terrestrial strata. Collectively, these new data sets permit evaluation of existing tectonic models of the evolution of the suture zone.

GEOLOGIC SETTING

Accreted Terranes, Accretionary Prism, and Volcanic Arcs

The inboard margins of the Insular terranes are juxtaposed against the Intermontane terranes (Fig. 1; Plafker and Berg, 1994), which consist mainly of Proterozoic–Paleozoic metamorphic rocks (Yukon-Tanana terrane) and adjacent arc-related rocks (Stikine terrane) that were accreted to the North American continental margin by Middle Jurassic time and perhaps much earlier (Foster et al., 1994; Dusel-Bacon et al., 2006; Beranek and Mortensen, 2011). The outboard margins of the Insular terranes are juxtaposed against the Chugach and Prince William terranes (Fig. 1), which consist of Jurassic–Cretaceous oceanic sedimentary and volcanic rocks interpreted as subduction complex deposits associated with northeastward/eastward subduction (modern coordinates) beneath the Insular terranes (Plafker et al., 1994; Amato et al., 2013). The magmatic record of subduction includes Jurassic–Cretaceous calc-alkaline plutons and volcanic rocks that crop out regionally within the Insular terranes (Moll-Stalcup, 1994; Plafker and Berg, 1994). In southern Alaska, these igneous products include the Early to Late Jurassic Talkeetna arc (Rioux et al., 2007), the Late Jurassic to Early Cretaceous Chitina arc (Plafker and Berg, 1994), and the Early Cretaceous Chisana arc (Barker et al., 1994). In southeastern Alaska and northern coastal British Columbia, arc plutons within the Insular terranes comprise the western Coast Mountains batholith (Gehrels et al., 2009; Cecil et al., 2011, 2018). The allochthonous Yakutat terrane is faulted against the outboard edge of the Chugach terrane and has been subducting at a shallow angle beneath the subduction complex and Insular terranes since Neogene time (e.g., Enkelmann et al., 2010; Worthington et al., 2012; Arkle et al., 2013).

Jurassic–Cretaceous Sedimentary Basins

Deformed Upper Jurassic and Lower Cretaceous marine sedimentary strata crop out for >1500 km along the inboard margin of the Insular terranes (Fig. 1; McClelland et al., 1992; Trop and Ridgway, 2007; Lowey, 2011). Western strata include the Kahiltna assemblage in south-central Alaska (Ridgway et al., 2002; Kalbas et al., 2007; Hults et al., 2013), whereas eastern strata consist of the Nutzotin, Dezadeash, and Gravina basins in eastern Alaska, Yukon Territory, and southeastern Alaska, respectively (Fig. 2; Berg et al., 1972; McClelland et al., 1992). Most studies interpret these basins to have formed in a retro-arc/back-arc position with respect to a northeastward/eastward-dipping subduction system, which is marked by Jurassic–Cretaceous plutons within the Insular terranes and metasedimentary strata in the Chugach accretionary complex (e.g., Trop and Ridgway, 2007; Yokelson et al., 2015). In these models, a second east-dipping subduction zone located along the eastern margin of the marine basins accommodated accretion of the Insular terranes and related marine basins (Trop and Ridgway, 2007, their figure 4); we favor this model. Alternatively, Sigloch and Mihalynuk (2013, 2017) interpreted the marine basins as part of a west-dipping subduction system to explain geophysical anomalies beneath eastern North America.

In south-central Alaska, the Kahiltna assemblage consists of Upper Jurassic and Lower Cretaceous marine clastic strata with an estimated thickness of ~3–5 km (Figs. 1 and 2; Ridgway et al., 2002). Sedimentologic analyses indicate that Kahiltna clastic strata represent chiefly marine mass-flow deposits that accumulated in submarine slope/fan environments (Kalbas et al., 2007; Hampton et al., 2007). U-Pb ages of detrital zircons indicate that Kahiltna

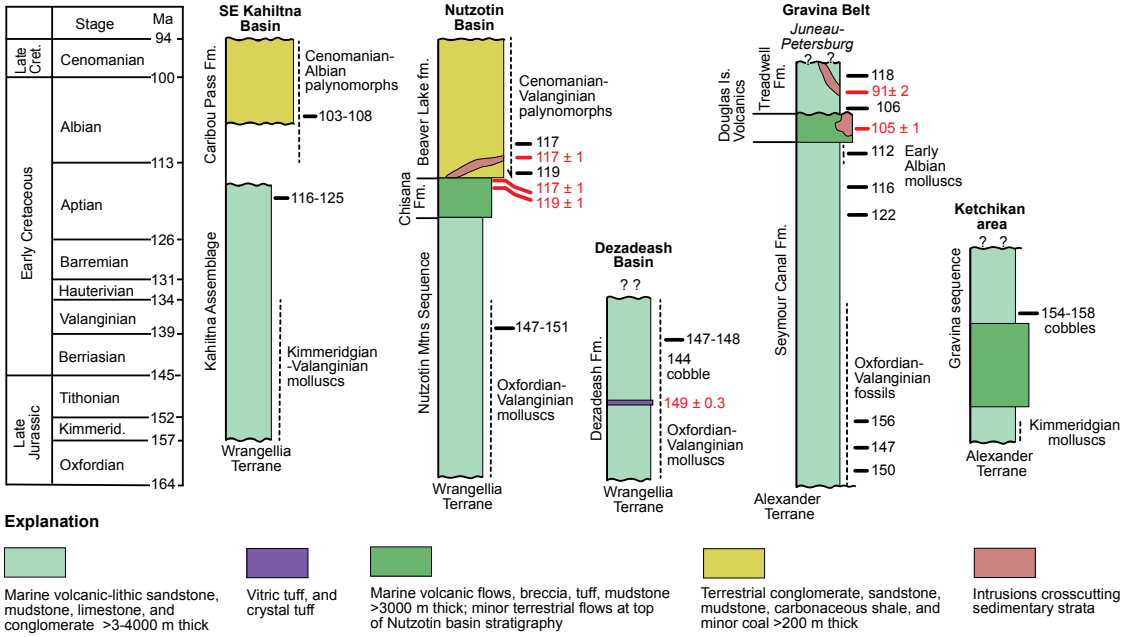

Figure 2. Generalized stratigraphy of Jurassic–Cretaceous basins along the inboard edge of the Insular terranes. Refer to Figure 1 for basin locations. Key age constraints include fossils (vertical dashed lines), igneous ages (red font), and the youngest populations of detrital zircons (black bold horizontal lines). Data sources: Ketchikan: Rubin and Saleeby (1991); Juneau-Petersburg: Berg et al. (1972), Gehrels (2000), Yokelson et al. (2015); Dezadeash: Lowey (2007, 2011, 2018); Nutzotin basin: Berg et al. (1972), Manuszak et al. (2007), this study; southeast Kahiltna basin (Talkeetna Mountains): Csejtey et al. (1992), Hampton et al. (2010, 2017). Stratigraphic positions of detrital zircon samples in the Dezadeash basin were estimated.

strata cropping out in the south accumulated along the northern margin of the Insular terranes in a back-arc position with respect to arc rocks within the Insular terranes (Hampton et al., 2010). Northern Kahiltna strata accumulated along the outboard (southern) margin of the Yukon-Tanana and Stikine terranes in a forearc setting (Hampton et al., 2010). The original width of the basin is controversial (for discussion, see Hults et al., 2013). Rocks mapped as part of the Kahiltna assemblage, consisting of argillite, greenstone, and chert, are interpreted as part of a south-facing accretionary wedge consisting of oceanic crust and hemipelagic sediment that formed prior to the final collapse of the Kahiltna basin (Bier and Fisher, 2003; Bier et al., 2017). Locally, marine strata of the Kahiltna assemblage experienced amphibolite-facies metamorphism at depths of ~25 km during Late Cretaceous time (Davidson et al., 1992). The metamorphic rocks, the mélange, and the submarine fan strata represent a zone of crustal thickening with south-verging contractional structures. Collectively, this zone of deformation has been referred to as the Alaska Range suture zone (Ridgway et al., 2002; Brennan et al., 2011; Trop et al., 2019) or mega–suture zone (Jones et al. 1982).

The Kahiltna assemblage is locally overlain by fluvial strata referred to as the Caribou Pass Formation (Fig. 2; Hampton et al., 2007). Maximum depositional ages from the fluvial strata of the Caribou Pass Formation range from ca. 108 to ca. 103 Ma, consistent with the presence of Albian–Cenomanian palynomorphs in the strata (Hampton et al., 2017). U-Pb ages and Hf isotope measurements indicate that the fluvial detritus was derived from both inboard and outboard magmatic provinces (e.g., Insular and Yukon-Tanana terranes), indicating that accretion against inboard terranes had taken place by Albian–Cenomanian time (Hampton et al., 2017).

In southeastern Alaska, the Gravina belt consists of Upper Jurassic and Lower Cretaceous marine clastic strata and mafic intermediate volcanic rocks with an estimated thickness of ~4 km (Figs. 1 and 2; Cohen and Lundberg, 1993). Maximum depositional ages derived from U-Pb zircon ages range from ca. 156 to ca. 106 Ma (Fig. 2; Gehrels, 2000; Yokelson et al., 2015). Intrusions with ca. 105–91 Ma U-Pb zircon ages crosscut Gravina belt strata locally (Fig. 2; Gehrels, 2000). U-Pb ages and Hf isotope determinations of detrital zircons indicate strata in the western portion of the Gravina belt accumulated along the inboard margin of the Alexander-Wrangellia terrane and in a back-arc position with respect to the western Coast Mountains batholith (Yokelson et al., 2015). Eastern Gravina belt strata accumulated along the western margin of the Stikine, Yukon-Tanana, and Taku terranes. The history of juxtaposition of western and eastern assemblages is obscured by subsequent plutonism, deformation, and metamorphism within the Coast Mountains orogeny (Gehrels et al., 2009; Cecil et al., 2011, 2018).

In the Yukon Territory, Late Jurassic and Early Cretaceous marine clastic and minor volcaniclastic strata of the Dezadeash Formation unconformably

overlie the eastern margin of Wrangellia along the north side of the Denali fault (Figs. 1 and 2; Dodds and Campbell, 1992). The lower and upper contacts of the Dezadeash Formation are not exposed; the formation is ~3 km thick (Lowey, 2007). Marine fossils in the Dezadeash Formation indicate deposition during Oxfordian to Valanginian time (Eisbacher, 1976a), consistent with the presence of a ca. 149 Ma tuff, a ca. 144 Ma igneous clast, and detrital zircons that indicate ca. 147–148 maximum deposition ages (Lowey, 2011, 2018). Deposition occurred chiefly in submarine slope/fan environments, as indicated by detailed lithofacies analyses (Lowey, 2007). Paleocurrents, compositional data, geochemical data, and detrital zircon ages indicate erosion of sources exclusively within the Insular terranes to the south (Lowey, 2011, 2018).

In eastern Alaska, Upper Jurassic to Lower Cretaceous marine clastic strata of the Nutzotin basin crop out along the south side of the Denali fault and depositionally overlie the inboard margin of Wrangellia (Figs. 1–3; Richter, 1976; Manuszak et al., 2007). The Nutzotin basin consists of a >6-km-thick succession of sedimentary and volcanic strata. Nutzotin basin strata include three distinct stratigraphic units, a lower marine sedimentary succession, a middle volcanic succession, and an upper, terrestrial sedimentary succession. The lower succession consists of the Nutzotin Mountains sequence, a >3-km-thick sequence of Upper Jurassic to Lower Cretaceous sandstone, conglomerate, and mudrock that depositionally overlies Triassic sedimentary strata of Wrangellia (Berg et al., 1972; Richter, 1976; Manuszak et al., 2007). Marine fossils indicate that deposition spanned Late Jurassic (Oxfordian) to Early Cretaceous (Valanginian) time, and lithofacies reflect deposition mainly in submarine slope/fan environments (Berg et al., 1972; Manuszak et al., 2007). Paleocurrents, conglomerate clast compositions, and detrital zircons ages reflect erosion of sources within Wrangellia to the south (Manuszak et al., 2007; Fasulo et al., 2018).

Depositionally overlying the Nutzotin Mountains sequence, the Lower Cretaceous Chisana Formation consists of a >3-km-thick succession of marine lava, volcanic breccia, tuff, and volcaniclastic sandstone (Berg et al., 1972; Richter and Jones, 1973; Short et al., 2005). The Chisana Formation has a gradational contact with Nutzotin Mountains sequence strata that bear Valanginian marine fossils (Richter and Jones, 1973; Manuszak, 2000). The lower 500 m section of the Chisana Formation yielded Hauterivian–Barremian fossils (Berg et al., 1972; Sandy and Blodgett, 1996). Two lavas sampled ~888 to ~1036 m above the base of the Chisana Formation yielded ca. 117–113 Ma $^{40}Ar/^{39}Ar$ ages (Short et al., 2005), although the age data and stratigraphic context were never formally published. Nearby cogenetic granitoid intrusions yielded ca. 126–113 Ma U-Pb zircon crystallization ages (Fig. 3; Graham et al., 2016) and 117–113 Ma $^{40}Ar/^{39}Ar$ cooling ages (Snyder and Hart, 2007). Geochemical compositions from the Chisana volcanic rocks and associated intrusions imply subduction-related arc magmatism (Barker et al., 1994; Short et al., 2005; Snyder and Hart, 2007).

Stratigraphically overlying the Chisana Formation volcanic deposits, previously unnamed

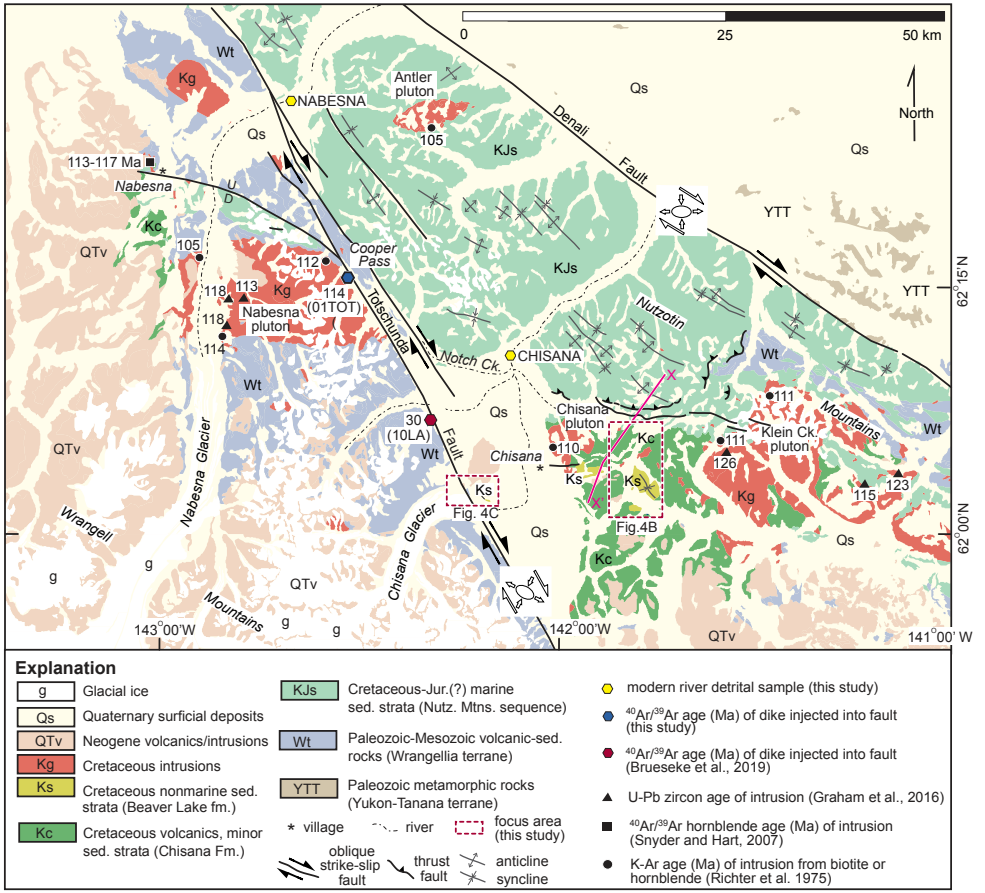

Figure 3. Geologic map of the eastern Alaska Range suture zone showing Jurassic–Cretaceous sedimentary, volcanic, and intrusive rocks within the suture zone between Wrangellia and the Yukon-Tanana terrane. Geology is adapted from Richter et al. (2006). Refer to Figure 1 for location.

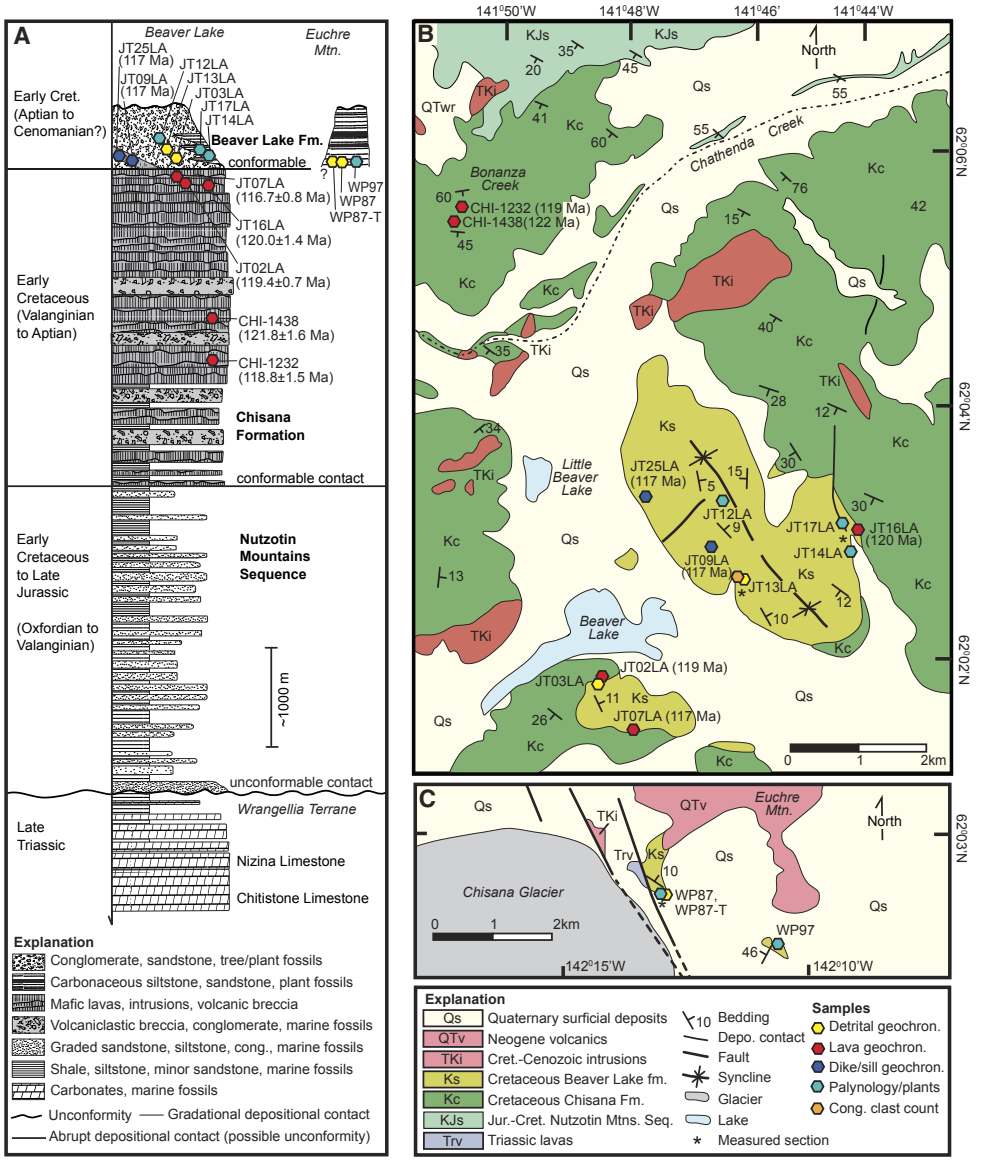

Figure 4. (A) Generalized stratigraphy and (B–C) geologic maps of the Beaver Lake (B) and Euchre Mountain (C) focus areas, showing sample locations and measured stratigraphic sections. Geology is from Richter (1971) and Richter and Jones (1973); Fm—Formation; Mtns—Mountains; Seq—sequence. *X* axis in A depicts weathering profile. Refer to Figure 3 for location.

conglomerate, sandstone, and mudrock (Ks map unit of Richter, 1976), are the primary focus of this paper. Outcrops of these strata are spatially limited, erosional remnants with preserved maximum thickness <200 m. Richter (1976) named the unit "Continental Sedimentary Rocks" but did not discuss depositional processes/environments. Richter (1976) inferred a Late Cretaceous(?) depositional age given that the strata depositionally overlie Barremian and older volcanic strata of the Chisana Formation (Richter and Jones, 1973). However, no direct age data have been reported from the terrestrial strata. A Cretaceous age is likely, given that Fiorillo et al. (2012) documented several dinosaur footprints. Fiorillo et al. (2012) inferred deposition in fluvial environments based on lithofacies and paleontologic observations. Based on our field studies, outcrops of the terrestrial strata north of Beaver Lake represent the thickest and most extensive outcrops and include the best-exposed depositional contacts with the underlying Chisana Formation (Fig. 4). Therefore, in this study we refer to the previously unnamed succession that overlies the Chisana Formation as the Beaver Lake formation in this report.

Based on stratigraphic similarities, the Dezadeash Formation and Nutzotin Mountains sequence are interpreted as part of the same depocenter that was dismembered and displaced dextrally ~370 km by the Denali fault since Early Cretaceous deposition (Figs. 1 and 2; Eisbacher, 1976b; Lowey, 1998). Other strike-slip faults like the Totschunda fault may have contributed to lateral shuffling of the marine basins (Waldien et al., 2018).

TOTSCHUNDA FAULT ZONE

The Totschunda fault bisects the Nutzotin basin (Figs. 1 and 3), including the western edge of the Beaver Lake formation. The Totschunda fault is an active oblique-slip fault, with significant historical right-lateral slip, as shown by the rupture pattern associated with the 2002 7.9 M Denali earthquake. Slip initiated on the previously unknown Susitna Glacier thrust fault and then propagated west to east along the Denali fault and then onto the

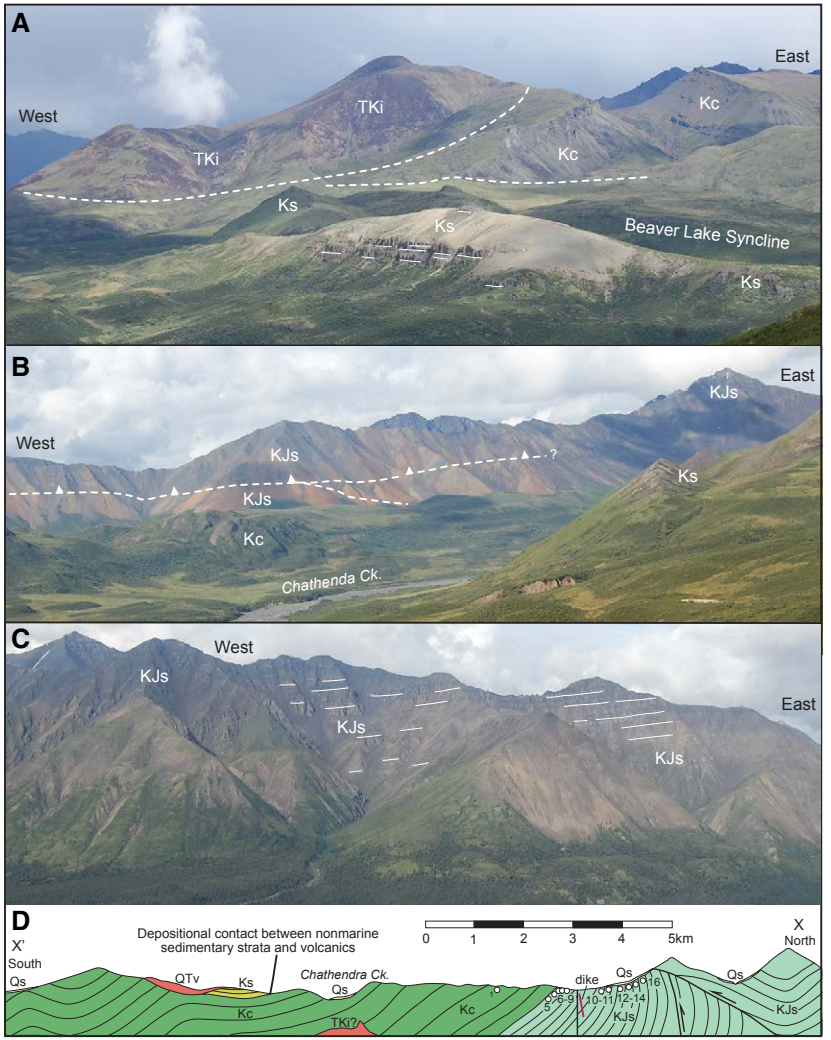

Figure 5. (A–C) Photographs and (D) cross section showing Cretaceous stratigraphic units of the Nutzotin basin, including Jurassic–Cretaceous marine sedimentary strata (KJs, Nutzotin Mountains sequence), Cretaceous volcanic rocks (Kc, Chisana Formation), and Cretaceous nonmarine strata (Ks, Beaver Lake formation). Solid white lines denote bedding orientation. Approximate lateral extent of photographs is (A) 2.2 km, (B) 5.2 km, and (C) 1.4 km. (A) Folded volcanic rocks (Kc) are overlain by gently dipping nonmarine sedimentary strata (Ks) near the axis of the Beaver Lake syncline. Volcanics are crosscut by a Cretaceous–Cenozoic intrusion (TKi). (B) Marine sedimentary strata (KJs) in background are juxtaposed above marine sedimentary strata (KJs) and volcanics (Kc) along north-dipping thrust fault (white dashed line with white triangles along the hanging wall). Gently dipping nonmarine sedimentary strata (Ks) overlie both units. (C) Gently dipping marine sedimentary strata (KJs) are exposed near Notch Creek. Exposed strata are >300 m thick. (D) Structural cross section showing depositional contacts between marine sedimentary (KJs), volcanic (Kc), and nonmarine sedimentary (Ks) successions. North-dipping thrust fault imbricates the marine sedimentary succession; thrust fault relationship is shown in photograph in B. Cross section was adapted from Richter and Jones (1973). Numbered white circles denote Early Cretaceous marine fossil localities summarized in Richter and Jones (1973). Refer to Figure 3 for cross-section location.

Totschunda fault (Eberhart-Phillips et al., 2003). Several possible inception ages and activity periods for the Totschunda fault have been proposed: early Cenozoic and possibly earlier (Goldfarb et al., 2013), middle Miocene (Trop et al., 2012), and middle Pleistocene (Richter and Matson, 1971; Plafker et al., 1977). A recent study by Brueseke et al. (2019) added to the debate. A dike that was injected into Totschunda fault gouge near Cross Creek (Fig. 3) yielded a ca. 29.7 ± 0.6 Ma $^{40}Ar/^{39}Ar$ age (Brueseke et al., 2019), implying the fault existed by early Oligocene time. New geophysical interpretations demonstrate substantial variations in seismic velocities across the Totschunda fault (Allam et al., 2017). Allam et al. (2017) inferred that the Totschunda fault separates two distinct crustal blocks, is located in an old and weak suture zone, and is likely a Cretaceous-aged structure.

Regional thermochronologic data support the Totschunda fault being a major structure since the Cretaceous. Apatite fission-track data from both sides of the Totschunda fault yield asymmetrical age patterns with old ages (ca. 145 Ma) on the east side of the fault and younger ages to the west of the fault (as young as ca. 25 Ma; Milde, 2014). Apatite fission-track ages increase westward away from the west side of the Totschunda fault to as old as ca. 95 Ma, indicating that the Totschunda fault controls localized exhumation patterns. HeFTy computational modeling indicated initiation of a period of rock cooling inferred to reflect exhumation along the Totschunda fault at ca. 90 Ma (Milde, 2014).

METHODS

Our analysis of the Beaver Lake and Chisana formations of the Nutzotin basin was based on field work and sampling from well-exposed outcrops at Euchre Mountain and Beaver Lake that were previously mapped (Richter 1971; Richter and Jones, 1973). Figures 3 and 4 show the generalized stratigraphy and geologic maps of the outcrops with key sample locations and measured stratigraphic sections. Figures 5 and 6 provide photographs of the stratigraphy.

Sedimentology

Lithofacies analysis of the Beaver Lake formation was carried out during targeted geologic mapping and stratigraphic section measuring. Individual beds were measured using a Jacob staff. Lithologies were denoted in terms of grain size, sedimentary structures, fossil content, bed geometry, and the nature of bed contacts. These data were grouped into lithofacies and lithofacies associations on the basis of grain size, lithology, and sedimentary structures.

Paleobotany

Abundant plant macrofossil remains were collected from loose float blocks; outcrops were not excavated to locate additional fossil remains. Plant fossil localities are depicted on Figure 3. Six mudstone samples were processed for plant microfossils, and those sample locations are depicted on Figure 3. Samples were processed twice as part of an internal quality control. Samples were processed by an independent laboratory (Global Geolab, Ltd.) and by Pierre Zippi (Biostratigraphy.com, LLC); the results were the same. The samples were washed to remove surficial contaminants. Carbonate minerals were dissolved using HCl, and silicate minerals were removed using HF. Organic residue was washed with cold HNO_3 followed by a wash with ammonia or KOH. Residues were then sieved through a 7 µm mesh screen to remove small particles that would be unidentifiable in transmitted light microscopy. Residues were then mounted on a coverslip with polyvinyl alcohol and fixed to a microscope slide with polyester resin. Pierre Zippi performed palynological, kerogen, and spore color analyses. Slides were examined with phase contrast and differential interference contrast illumination using oil immersion at a minimum of 500× with a research-grade Zeiss Axio Imager microscope. Age interpretations for most samples were based on palynology and were integrated with published studies as well as a proprietary regional database compiled and maintained by Biostratigraphy.com.

$^{40}Ar/^{39}Ar$ Geochronology

Traditional methods of crushing, sieving, washing, and handpicking were used to separate phenocryst-free whole-rock chips and hornblende from lava and intrusion samples for incremental step-heating analysis, detrital hornblende from a sandstone sample for single-grain fusion analysis, and alkali feldspar from an alkali feldspar syenite dike for incremental step-heating analysis. The $^{40}Ar/^{39}Ar$ age determinations were performed at the Geochronology Facility at the University of Alaska–Fairbanks. The monitor mineral MMhb-1 (Samson and Alexander, 1987), with an age of 523.5 Ma (Renne et al., 1994), was used to monitor neutron flux (and calculate the irradiation parameter, *J*). The samples and standards were wrapped in aluminum foil and loaded into aluminum cans of 2.5 cm diameter and 6 cm height. The samples were irradiated in position 5c of the uranium-enriched research reactor at McMaster University in Hamilton, Ontario, Canada, until exposed to 20 megawatt-hours. Upon their return from the reactor, the samples and monitors were loaded into 2-mm-diameter holes in a copper tray that was then loaded in an ultrahigh-vacuum extraction line. The monitors were fused, and samples heated, using a 6 W argon-ion laser following the technique described in York et al. (1981), Layer et al. (1987), and Layer (2000). Argon purification was achieved using a liquid nitrogen cold trap and a SAES Zr-Al getter at 400 °C.

Samples were analyzed in a VG-3600 mass spectrometer at the Geophysical Institute, University of Alaska–Fairbanks. The argon isotopes measured were corrected for system blank and mass discrimination, as well as calcium, potassium, and chlorine interference reactions following procedures outlined in McDougall and Harrison (1999). Typical full-system 8 min laser blank values (in moles) were generally 2×10^{-16} mol ^{40}Ar, 3×10^{-18} mol ^{39}Ar, 9×10^{-18} mol ^{38}Ar, and 2×10^{-18} mol ^{36}Ar, which are 10–50 times smaller than the sample/standard volume fractions. Correction factors for nucleogenic interferences during irradiation were determined from irradiated CaF_2 and K_2SO_4 as follows: $(^{39}Ar/^{37}Ar)Ca = 7.06 \times 10^{-4}$, $(^{36}Ar/^{37}Ar)Ca = 2.79 \times 10^{-4}$, and $(^{40}Ar/^{39}Ar)K = 0.0297$. Mass discrimination was monitored by running calibrated air shots. The mass discrimination during these experiments was 1.3% per mass unit. While doing our experiments, calibration measurements were made on a weekly to monthly basis to check for changes in mass discrimination; no significant variation was observed during these intervals. Supplemental Item C[1] summarizes the $^{40}Ar/^{39}Ar$ results, with all ages quoted to the ± 1σ level and calculated using the constants of Renne et al. (2010). The integrated age is the age given by the total gas measured and is equivalent to a potassium-argon (K-Ar) age. The spectrum provides a plateau age if three or more consecutive gas fractions represent at least 50% of the total gas release and are within two standard deviations of each other (mean square weighted deviation < 2.5).

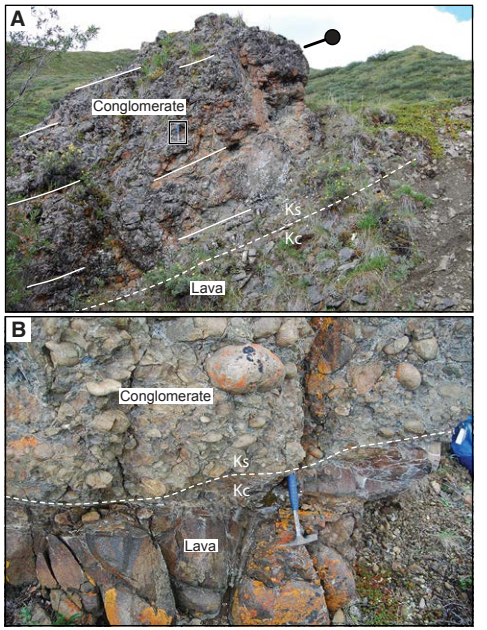

Figure 6. Photographs showing depositional contact between lavas of the uppermost Chisana Formation (Kc) and basal conglomerate of the Beaver Lake formation (Ks) near Beaver Lake. Solid white line denotes bedding orientation. Dashed white line denotes location of contact between lava and basal conglomerate. Refer to Figure 4 for locations; A is near JT16LA, and B is at JT07LA.

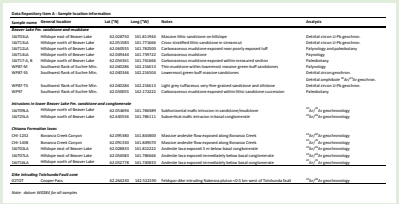

[1]Supplemental Items. Item A: Sample location information. Item B: Palynological results from Beaver Lake formation mudstone. Item C: $^{40}Ar/^{39}Ar$ analytical results from Cretaceous volcanic and intrusive rocks underlying and intruding the Beaver Lake formation, detrital hornblendes from Beaver Lake formation sandstone, and a Totschunda fault zone dike. Item D: U-Pb analytical results from detrital zircons from Beaver Lake formation sandstone. Please visit https://doi.org/10.1130/GES02127.S1 or access the full-text article on www.gsapubs.org to view the Supplemental Items.

U-Pb Geochronology

Zircon grains were separated using standard mineral separation techniques at Bucknell University and the University of Arizona. Special care was taken throughout sample processing to avoid biasing the final separate of zircon grains by size, shape, color, degree of rounding, etc. Grains were mounted in a 1 in. (2.5 cm) epoxy mount alongside fragments of standard zircons. Mounts were polished to a 1 μm finish, imaged using cathodoluminescence (CL) and/or backscattered electron (BSE) methods, and cleaned with a 2% HNO_3 and 1% HCl solution prior to isotopic analysis. CL and BSE images were used to select analytical points, avoiding complex internal structures and fractures. Additionally, images provided a qualitative analysis of grain textures, morphology, internal zoning patterns, and variations in CL color response. U-Pb geochronologic analyses of zircon grains were conducted by laser ablation–multicollector–inductively coupled plasma–mass spectrometry at the University of Arizona LaserChron Center. Zircon crystals were randomly selected for analysis, irrespective of size, shape, color, and degree of rounding; grains with visible cracks or inclusions were avoided. After every fourth or fifth measurement of an unknown zircon, analyses were calibrated against a measurement of a Sri Lanka zircon standard (563 ± 3.2 Ma; Gehrels et al., 2008). The $^{207}Pb/^{235}U$ and $^{206}Pb/^{238}U$ ratios and apparent ages were calculated using the Isoplot software program (Ludwig, 2008). Supplemental Item D (footnote 1) summarizes the U-Pb results. The systematic uncertainty, which includes contributions from the standard calibration, the age of the calibration standard, the composition of common Pb, and the ^{238}U decay constant, was 1%–2%, based on similar analyses (Gehrels et al., 2008). The data were filtered according to precision (typically 10% cutoff) and discordance (typically 30%) and then plotted on Pb/U concordia diagrams.

SEDIMENTOLOGIC RESULTS

Table 1 summarizes the individual lithofacies documented in the field and corresponding standard interpretations of physical and depositional processes. Measured stratigraphic sections (Fig. 7) and photographs (Fig. 8) graphically depict representative lithofacies. Thus, we provide only a brief description of the lithofacies that comprise two lithofacies associations here.

Gravelly Lithofacies Association

This association consists chiefly of massive to imbricated, clast-supported pebble-cobble

TABLE 1. LITHOFACIES CHARACTERISTICS AND INTERPRETATIONS FOR BEAVER LAKE FORMATION, EASTERN ALASKA

Facies	Color, bedding, texture, structures, fossils	Facies interpretations
Gmm	Massive granule to cobble conglomerate with minor boulders, poorly to moderately sorted, mostly subrounded volcanic clasts; matrix supported with fine- to medium-grained sandstone and mudstone matrix; unstratified; wood and leaf fragments.	Debris-flow and hyperconcentrated flood flow in shallow fluvial channels and bar tops (Pierson and Scott, 1985; Smith, 1986)
Gcm	Massive, granule-pebble-cobble conglomerate with moderately sorted, mostly subrounded clasts; clast-supported with medium- to coarse-grained sandstone matrix; unstratified to crudely horizontally stratified with scours; wood and plant fragments.	Deposition by traction currents in unsteady streamflow and high-concentration flood flow in shallow fluvial channels and bar tops (Pierson and Scott, 1985; Smith, 1986)
Gcmi	Imbricated, pebble-cobble conglomerate with moderately to well-sorted, mostly subrounded clasts; clast-supported with medium- to coarse-grained sandstone matrix; unstratified to crudely horizontally stratified; wood and plant fragments.	Deposition by traction currents in unsteady streamflow and high-concentration flood flow in shallow fluvial channels and bar tops (Miall, 1978; Collinson, 1996)
Sm	Gray to tan, fine- to coarse-grained, massive lithic sandstone, scours, granule-pebble stringers, plant debris, petrified to coalified wood fragments; medium to thick bedded.	Streamflow and high-concentration flood flow in shallow fluvial channels and bar tops and crevasse splays (Miall, 1978; Collinson, 1996)
Sh	Gray to tan, fine- to coarse-grained, plane-parallel laminated lithic sandstone, plant debris, and petrified to coalified wood; medium to thick bedded.	Deposition under upper plane bed conditions from very shallow or strong (>1 m/s) unidirectional flow conditions in fluvial channels, bar tops, crevasse channels, and sheetfloods (Miall, 1978)
Sp	Gray to tan, fine- to coarse-grained, planar cross-stratified lithic sandstone with thin granule-pebble stringers, plant debris, and petrified to coalified wood; medium to thick bedded.	Migration of 2D ripples and small dunes under moderately strong (~40–60 cm/s) unidirectional channelized flow in fluvial channels, bar tops, crevasse channels (Miall, 1978)
St	Gray to tan, fine- to coarse-grained, trough-cross-stratified lithic sandstone with thin granule-pebble stringers, plant debris, and petrified to coalified wood; medium to thick bedded.	Migration of 3D ripples and dunes under moderately strong (40–100 cm/s), unidirectional channelized flow in fluvial channels, bar tops, crevasse channels (Miall, 1978)
Sr	Gray to tan, fine- to medium-grained lithic sandstone with asymmetric two- (2D) and three-dimensional (3D) current ripples; plant debris and petrified to coalified wood; thin to medium bedded.	Migration of 2D and 3D ripples under weak (20–40 cm/s) unidirectional flow in shallow fluvial channels, bar tops, crevasse channels, and lake margins (Miall, 1978)
Fsm	Gray siltstone with fragmented plant fossils, coalified wood fragments, organic debris, root traces, sparse evidence of pedogenesis, mainly mottling and bioturbation.	Suspension fallout and pedogenesis in poorly drained, vegetated floodplains/wetlands (Collinson, 1996; Miall, 2006; Melchor, 2007)
Fsl	Gray and green-gray laminated siltstone and shale, minor rootlets, delicately preserved fossil plant leaves, stems, and seeds.	Subaqueous suspension settling in low-energy floodplain ponds/lakes (Johnson and Graham, 2004; Pietras and Carroll, 2006)
Fsc	Dark gray to black carbonaceous mudstone and rare stringers of blocky lignite, coalified organic matter, root traces, delicately preserved fossil plant leaves, plant leaf mats, and comminuted plant debris.	Suspension settling and accretion of decaying organic matter and clastic mud in poorly drained floodplain wetlands (small bogs, fens, moors, muskegs, or swamps; McCabe, 1984, 1991)
Vt	Tan reworked tuff and tuffaceous siltstone with subangular framework grains of pumice, feldspar, and quartz; laminated to massive with rootlets and organic debris.	Pyroclastic fallout deposition and minor reworking and pedogenic overprinting (Cas and Wright, 1987)

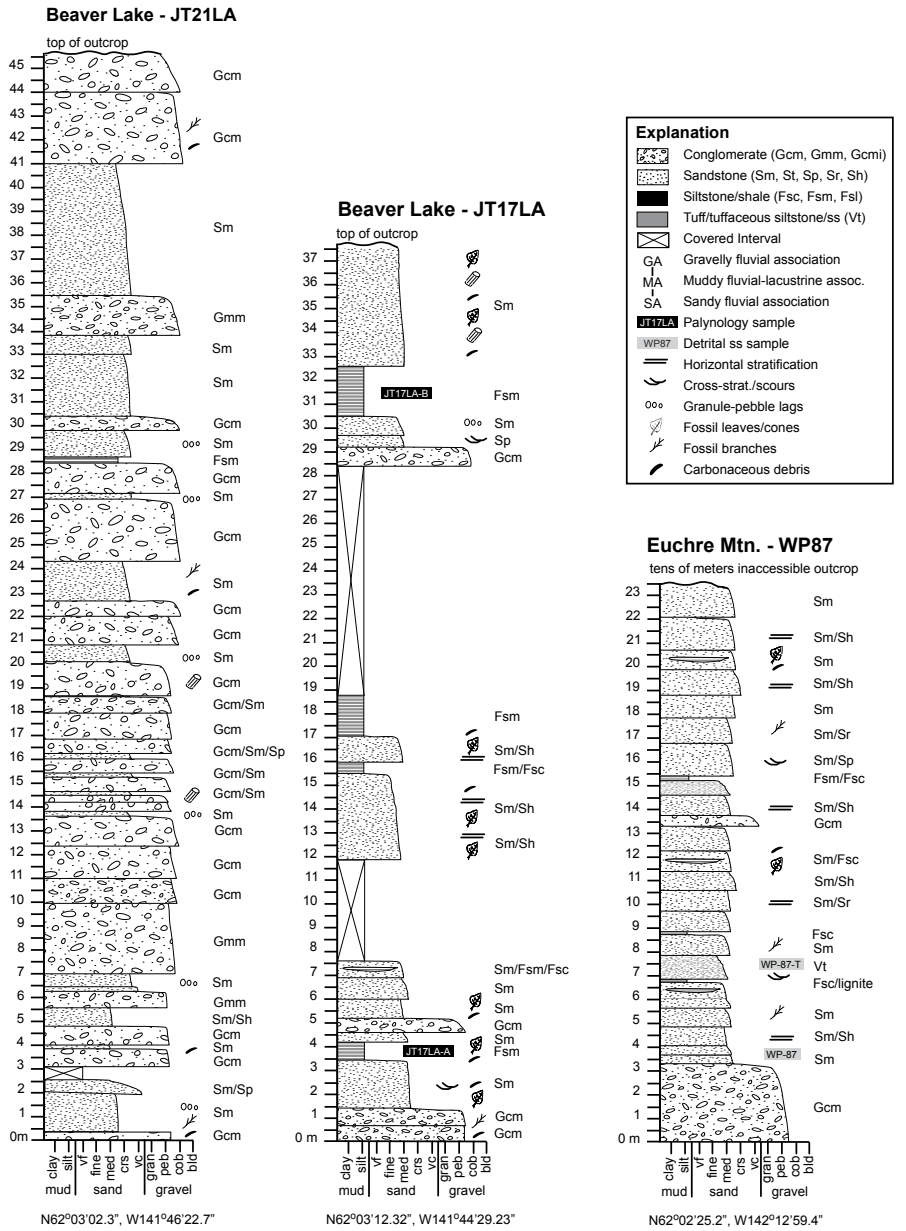

Figure 7. Detailed logs (in m) of measured stratigraphic sections of Cretaceous sedimentary strata spanning the Beaver Lake formation in eastern Alaska. Refer to Figure 4 for section locations and Table 1 for explanation of lithofacies abbreviations (ss—sandstone). Grain-size abbreviations: vf—very fine; crs—coarse; vc—very coarse; gran—granule; peb—pebble; cob—cobble; bld—boulder.

conglomerate (lithofacies Gcm, Gcmi) and subordinate matrix-supported pebble-cobble-boulder conglomerate (Gmm), massive to horizontally stratified lithic sandstone (Sm, Sh), and siltstone (Sm, Sh, Fsm) (Table 1; section JT21LA on Fig. 7; Figs. 8A–8C). Individual packages of conglomerate are laterally discontinuous over several meters to >20 m and are typically >0.5–3 m thick. Laterally discontinuous sandstone and siltstone interbeds are typically <50 cm thick and ~3–8 m wide. Most conglomerates consist of subrounded clasts that are moderately sorted and contained in medium- to coarse-grained lithic sandstone. Most conglomerate and sandstone beds are amalgamated into 5–20-m-thick successions that crudely fine upward. Conglomerates contain petrified wood fragments, whereas interbedded sandstone and mudrock yield plant leaves and stems. Upright tree trunks >2 m tall are preserved locally within conglomerate-sandstone packages.

Sandy-Muddy Lithofacies Association

This association is characterized by diverse sandstone and mudrock lithofacies with sparse conglomerate. Amalgamated successions of lenticular beds of massive, cross-stratified, and horizontally stratified lithic sandstone (Sm, Sp, St, Sh) and minor conglomerate (Gcm, Gcmi) occur in association with finer-grained packages of thin-bedded carbonaceous siltstone and shale (Fsl, Fsm, Fsc) and sparse thin-bedded, upward-fining units of massive to horizontal- and ripple-laminated sandstone (Sm, Sh, Sr; Table 1; section JT17LA and WP87 on Fig. 7; Figs. 8D–8F). Individual packages of sandstone are laterally discontinuous over several meters to tens of meters and are typically 0.5–3 m thick. Amalgamated sandstone successions range from hundreds-of-meters-thick packages with sparse mudrock to successions a few meters thick that fine abruptly or gradually upward into mudstone successions meters to tens of meters thick. Sparse bioturbation and rootlets (rhizoliths) reflect pedogenesis within the mudrock intervals. Features indicative of persistent desiccation of soil (i.e., caliche nodules, pedogenic slickensides) were not observed. Variably

preserved plant remains occur in all lithofacies; siltstone and shale yield especially well-preserved plant remains. Charcoal is abundant locally in siltstone.

PALEOBOTANICAL RESULTS

Limited taxonomic information has been reported for the abundant paleofloral remains in the Beaver Lake formation (Fiorillo et al., 2012). New macrofloral and microfloral data shed light on the age and depositional environments.

Macroflora

The fossil macroflora recovered from the Beaver Lake formation includes foliage of predominantly polypodiaceous ferns and cupressaceous conifers, a cone of the family Pinaceae, carbonized root traces, and unidentified gymnosperm wood. No angiosperm macrofossil material was recovered.

Fern foliage is preserved as partial frond compressions with some specimens exhibiting pinnule venation. The collection includes ferns comparable with *Asplenium* sp. (Fig. 9A), *Cladophlebis* sp. (Fig. 9B), and *Birisia* sp. (Fig. 9C; Hollick, 1930; Spicer et al., 2002; Spicer and Herman, 2002). Most conifer foliage is within the Cupressaceae, including proximal and distal branch leaves of cf. *Sequoia* sp. (Fig. 9D), *Cryptomeria* sp. (Fig. 9E), cf. *Widdringtonites* sp. (Fig. 9F), a variety of foliar forms similar to cf. *Taiwania* sp. (Fig. 9G), and *Elatocladus* sp. (Fig. 9H; Hollick, 1930; Spicer et al. 2002; Spicer and Herman, 2002; LePage, 2009;

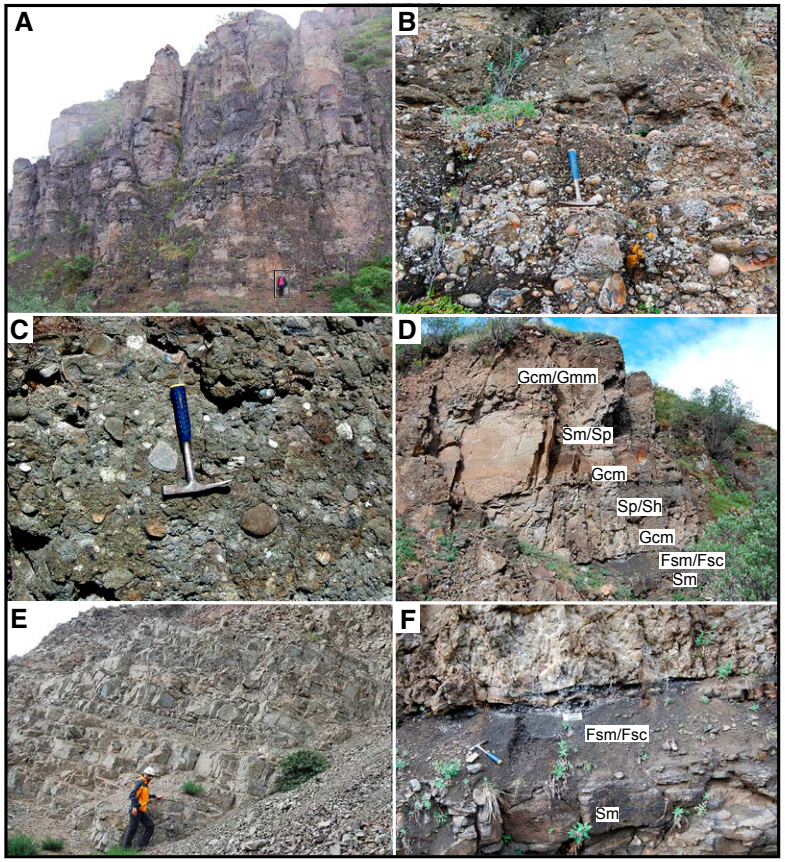

Figure 8. Photographs of (A–C) gravelly lithofacies at Beaver Lake section JT21LA, (D, F) Beaver Lake section JT17LA, and (E) sandy/muddy lithofacies at Euchre Mountain section WP87. Refer to Table 1 for lithofacies code abbreviations. (A) Amalgamated conglomerate and sandstone succession with person for scale (lower right). (B–C) Moderately sorted subrounded clasts in pebble-cobble conglomerate with variable degrees of clast support. Note upward fining in B. (D) Sandstone (Sm, Sp) and conglomerate succession (Gcm, Gmm) overlying dark mudrock (Fsm, Fsc). Outcrop is 12 m tall. (E) Amalgamated lenticular sandstone beds. (F) Carbonaceous siltstone (Fsc) and massive siltstone (Fsm) among massive sandstone units (Sm).

Figure 9. Photographs of paleofloral remains from the Beaver Lake formation at Euchre Mountain and Beaver Lake. (A) *Asplenium* sp. (WP87CS-13A); (B) *Cladophlebis* sp. (WP87CS-02A); (C) *Birisia*? sp. (WP87CS-15A); (D) cf. *Sequoia* sp. (WP87CS-13B); (E) cf. *Cryptomeria* sp. (JT17LA-5A); (F) cf. *Widdringtonites* sp. (WP87–17A); (G) cf. *Taiwania* sp. (WP87CS-04A); (H) *Elatocladus*? sp. (WP87–16A); (I) Pinaceae cone (JT17LA-1); (J) root traces (WP87). All scales 1 cm.

Herman and Sokolova, 2016). Other foliage fragments observed in the collected samples are putatively assigned here to the conifer form *Podozamites*. The lone cone fossil (Fig. 9I) is preserved in three dimensions and is most similar to those of modern *Picea*. The gymnosperm wood is poorly permineralized and unidentifiable to family. The floral remains at both Euchre Mountain and Beaver Lake are often preserved at angles to bedding, suggesting incorporation into fluvial deposits in an active flood basin. Despite this, however, the articulated preservation of many foliage forms suggests that the material was not delivered from a great distance.

Microflora

Samples from the Beaver Lake section yielded sparse identifiable palynomorphs, and samples from the Euchre Mountain section were barren of identifiable palynomorphs. The paucity of identifiable palynomorphs from the sampled outcrops is attributable to the high thermal maturity resulting from mid-Cretaceous to Cenozoic intrusions and lavas that crop out among the sampled outcrops (Fig. 4). The recovered palynomorphs from the Beaver Lake section include *Cicatricosisporites* sp. (B–F on Fig. 10), *Osmundacidites wallmani*, *Classopollis* sp. (G–H on Fig. 10), *Distaltriangulisporites perplexus* (K–M on Fig. 10), *Matonisporites crassiangulatus* (P–R on Fig. 10), and *Deltoidospora minor*. Samples from the Beaver Lake section yielded chiefly dark wood kerogen (unstructured blocky, structured tracheids, charcoal), perforate kerogen typical of high thermal maturity, and very rare amorphous kerogen. Refer to Supplemental Item B (footnote 1) for palynological details.

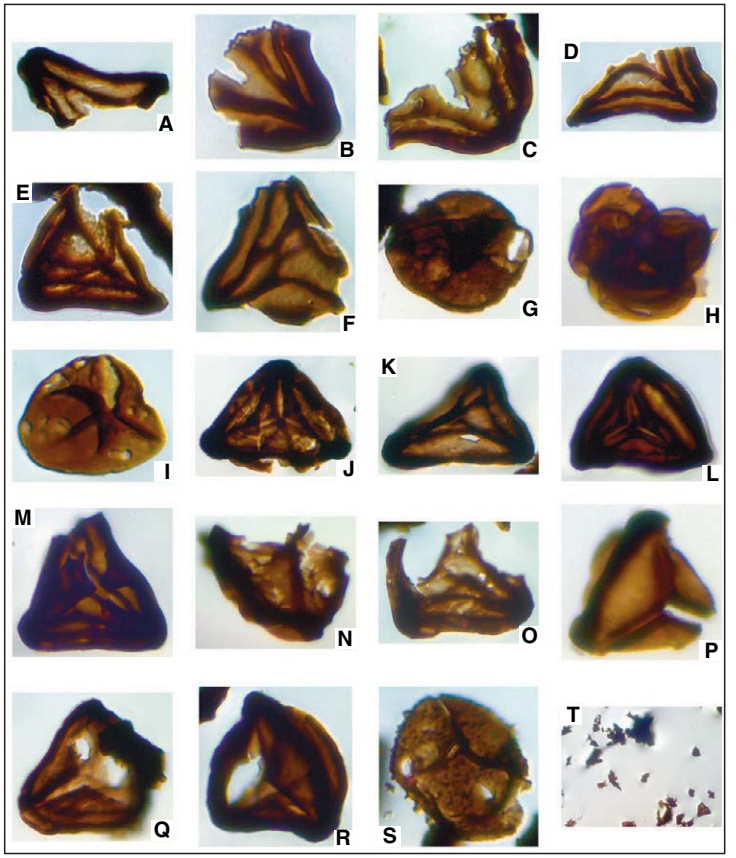

Figure 10. Photographs of key pollen and spores recovered from Beaver Lake formation mudstone samples at Beaver Lake. (A) *Cicatricosisporites* or *Distaltriangulisporites* fragment?; (B–F) *Cicatricosisporites* sp. fragment; (G) *Classopollis* sp.?; (H) *Classopollis*? sp. tetrad; (I) *Deltoidospora* minor; (J) *Distaltriangulisporites costatus* or *perplexus*; (K–M) *Distaltriangulisporites perplexus*; (N–O) possibly *Distaltriangulisporites*; (P–R) *Matonisporites crassiangulatus*, triangular with valvae; (S) *Neoraistrikia* truncate; (T) mature kerogen (wood). Image scales are A: 55 µm, B: 29 µm, C: 40 µm, D: 42 µm, E: 40 µm, F: 32 µm, G: 35 µm, H: 32 µm, I: 34 µm, J: 63 µm, K: 48 µm, L: 40 µm, M: 40 µm, N: 41 µm, O: 43 µm, P: 35 µm, Q: 45 µm, R: 44 µm, S: 35 µm, T: 475 µm.

GEOCHRONOLOGICAL AND COMPOSITIONAL RESULTS

The $^{40}Ar/^{39}Ar$ geochronology of lavas and intrusions provided constraints on the timing of deposition, magmatism, and deformation. Conglomerate compositional data, U/Pb geochronology of detrital zircons, and $^{40}Ar/^{39}Ar$ geochronology of detrital amphiboles permitted reconstruction of sediment provenance and constraints on the maximum timing of deposition. The $^{40}Ar/^{39}Ar$ age uncertainties are at the ±1σ level. Refer to Figure 4 for sample locations and Supplemental Item A (footnote 1) for sample details. Refer to Table 2 for a summary of $^{40}Ar/^{39}Ar$ ages and Supplemental Item C for $^{40}Ar/^{39}Ar$ analytical results. Refer to Supplemental Item D for U-Pb analytical results.

Conglomerate Composition

Compositional data were obtained from counting 104 individual clasts from a conglomerate bed

TABLE 2. SUMMARY OF $^{40}Ar/^{39}Ar$ ANALYTICAL RESULTS FROM CHISANA FORMATION (FM) LAVAS AND INTRUSIONS

Sample	Rock unit	Phase analyzed	Integrated age (Ma)	Plateau age (Ma)	Plateau information	Isochron age (Ma)	Isochron or other information
CHI-1232	Chisana Fm. lava	HBL	113.8 ± 0.5	**118.8 ± 1.5**	6 out of 14 fractions 88.4% ^{39}Ar release MSWD = 0.88	—	—
CHI-1438	Chisana Fm. lava	WR	124.9 ± 2.2	**121.8 ± 1.6***	3 out of 8 fractions 44.0% ^{39}Ar release MSWD = 0.14	—	—
16JT02LA	Chisana Fm. lava	WR	120.6 ± 0.7	**119.4 ± 0.7**	5 out of 8 fractions 63.0% ^{39}Ar release MSWD = 1.37	120.1 ± 0.6	5 of 8 fractions $^{40}Ar/^{36}Ar_i$ = 289.3 ± 3.6 MSWD = 0.64
16JT07LA	Chisana Fm. lava	WR	118.5 ± 0.6	**116.7 ± 0.8***	3 out of 8 fractions 47.5% ^{39}Ar release MSWD = 2.45	—	—
16JT16LA	Chisana Fm. lava	WR	118.8 ± 1.5	**120.0 ± 1.7**	6 out of 10 fractions 68.0% ^{39}Ar release MSWD = 1.48	121.4 ± 4.4	6 of 10 fractions $^{40}Ar/^{36}Ar_i$ = 293.5 ± 7.3 MSWD = 1.80
16JT09LA	Intrusion in lower Beaver Lake fm	WR	117.9 ± 0.6	**116.8 ± 0.6**	4 out of 8 fractions 54.5% ^{39}Ar release MSWD = 0.13	116.1 ± 1.8	4 of 8 fractions $^{40}Ar/^{36}Ar_i$ = 303.6 ± 24.2 MSWD = 0.09
16JT25LA	Intrusion in lower Beaver Lake fm	WR	117.8 ± 0.6	**117.1 ± 0.8***	5 out of 8 fractions 44.6% ^{39}Ar release MSWD = 0.43	115.7 ± 1.3	5 of 8 fractions $^{40}Ar/^{36}Ar_i$ = 303.1 ± 7.3 MSWD = 0.43
01TOT	Dike in Totschunda fault	KSP	113.8 ± 1.1	**113.8 ± 1.3**	12 of 14 fractions 98.7% 39Ar release MSWD = 1.41	113.8 ± 1.2	14 of 14 fractions $^{40}Ar/^{36}Ar_i$ = 277.3 ± 10.1 MSWD = 0.70

Note: Samples were analyzed with standard MMhb-1 with an age of 523.5 Ma. Most robust age determination is in bold. Refer to Supplemental Item B (see text footnote 1) for supplemental plots and analytical data. Uncertainties are 1σ. WR—whole-rock, HBL—hornblende, KSP—feldspar, MSWD—mean square of weighted deviates.
*Did not meet all the criteria for a plateau age, and so a weighted average age determination is presented.

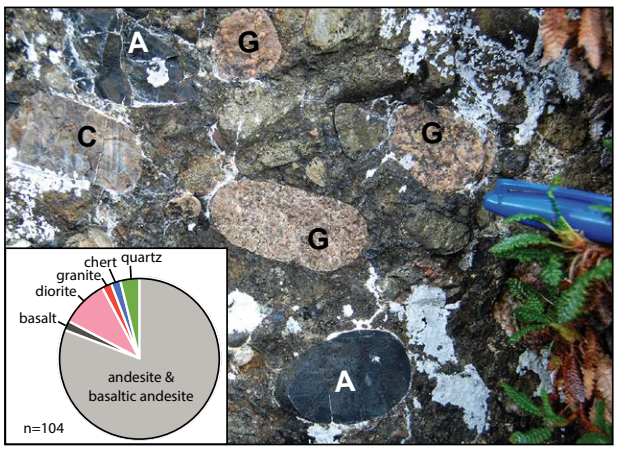

Figure 11. Photograph of common clast types in Beaver Lake formation conglomerate, mainly dark-gray andesite (A), pink granite (G), and gray chert (C) clasts. Pen cap for scale. Inset: Histograms of clast compositions of Beaver Lake formation conglomerates showing dominance of volcanic-plutonic clast lithologies. Refer to Figure 4 for location (JT13LA); *n*—total number of clasts counted.

at Beaver Lake (Fig. 4). Clasts were identified in the field by tabulating the lithology of all gravel-sized clasts within a 1–5 m² outcrop face to provide statistical significance (van der Plas and Tobi, 1965). Clasts counted were green-gray, aphanitic to porphyritic andesite (81%); dark-gray to black basalt (2%); medium- to coarse-grained gray diorite (9%); coarse-grained pink granite (2%); black/gray chert (2%); and white quartz (4%; Fig. 11).

Detrital Amphiboles

Detrital amphiboles were extracted from a sandstone sampled in the lowermost Beaver Lake formation at Euchre Mountain (Figs. 4 and 8). The sampled sandstone is moderately to poorly sorted and medium to coarse grained with abundant

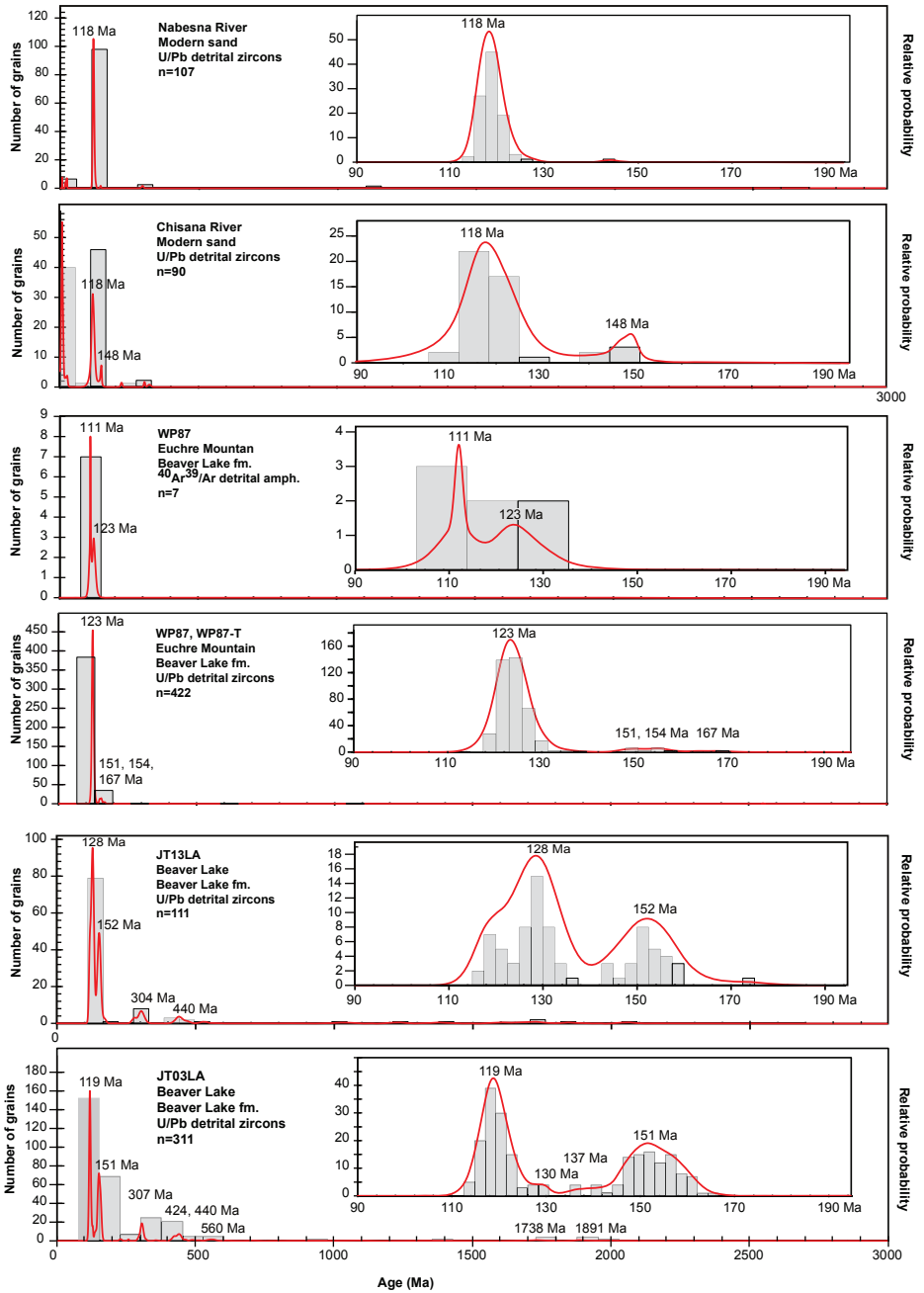

volcanic-lithic fragments, pyroxenes, and amphiboles. The amphiboles yielded Cretaceous $^{40}Ar/^{39}Ar$ ages that define ca. 111 Ma and ca. 123 Ma age peaks (WP87 on Fig. 12). The youngest cluster of overlapping amphibole ages was ca. 111 Ma (Table 3).

Detrital Zircons

Detrital zircons were separated from four sandstones sampled in the Beaver Lake formation at Beaver Lake and Euchre Mountain (Figs. 4 and 8). Sampled sandstones are moderately to poorly sorted, medium-grained volcanic-lithic sandstones with abundant plagioclase feldspar, clinopyroxene, and amphibole. Detrital zircons from two sandstone samples at Euchre Mountain yielded chiefly Cretaceous U/Pb ages and a dominant age peak of ca. 123 Ma (Fig. 12). Subordinate age peaks were Jurassic and ranged from ca. 151 to ~167 Ma. The youngest clusters of overlapping ages were ca. 123 Ma (Table 3). Detrital zircons from two Beaver Lake formation sandstones at Beaver Lake yielded chiefly Cretaceous ages (ca. 119 Ma and ca. 128 Ma age peaks on Fig. 12). Subordinate age peaks were Jurassic, Pennsylvanian, Silurian, and Proterozoic. The youngest clusters of overlapping ages were observed ca. 119–117 Ma (Table 3).

We also report U-Pb zircon ages from modern sand from the Nabesna and Chisana Rivers, which drain Wrangellia along the north flank of the Wrangell Mountains (Fig. 3). These modern river sands yielded chiefly Cretaceous ages (ca. 118 Ma age peak) and subordinate Jurassic (ca. 148 Ma age peak) and Neogene ages (Fig. 12).

Figure 12. Histograms (light-gray bars) and age probability diagrams (red curves) for detrital zircon and amphibole ages from Beaver Lake formation samples and sand from modern rivers in the study area. Age determinations represent individual spot analyses of separate zircons or amphiboles. Each curve is the sum of ages and uncertainties from all analyses of a set of samples. The area under each curve was normalized according to the number of constituent analyses (Gehrels, 2012, 2014). Peaks in age probability are shown for each set of samples. Inset probability plots show details of main age population. Refer to Figures 3 and 4 and Supplemental Item A (text footnote 1) for sample locations.

TABLE 3. DEPOSITIONAL AGES AND AGE SPAN OF THE BEAVER LAKE FORMATION INFERRED FROM DETRITAL GEOCHRONOLOGY, IGNEOUS GEOCHRONOLOGY, AND BIOSTRATIGRAPHY

Sample	Underlying lava ages	Detrital ages							Biostratigraphic age		Inferred depositional age
			Youngest consecutive peak			Unmix		Y3G			
	Age (Ma)	Mineral	Weighted mean age (Ma)	*n*	MSWD	Youngest age (Ma)	Misfit	Age (Ma)	Stage or Period	Age (Ma)	Age (Ma)
Beaver Lake area											
16JT13LA	**120.0 ± 1.4**	Zircon	125.3 ± 1.5	52	1.6	125.8 ± 0.5	0.47	**117.0 ± 3.7**	L. Val. to E. Cen.	**Ca. 137 to ca. 98**	Ca. 117 Ma to >98 Ma
16JT03LA	**119.4 ± 0.7, 116.7 ± 0.8**	Zircon	119.5 ± 0.6	120	2.6	**118.8 ± 0.2**	**0.74**	113.2 ± 2.7	L. Val. to E. Cen.	**Ca. 137 to ca. 98**	Ca. 117 Ma to >98 Ma
Euchre Mountain area											
WP87-SS	–	Amphibole	**111.3 ± 0.8**	**4**	**0.36**	No solution		111.3 ± 1.7	Cretaceous	**Ca. 145 to ca. 66**	Ca. 111 Ma to >66 Ma
WP87-SS	–	Zircon	**123.2 ± 0.8**	**108**	**0.32**	123.3 ± 0.4	1	118.5 ± 4.6	Cretaceous	**Ca. 145 to ca. 66**	Ca. 123 Ma to >66 Ma
WP87-TS	–	Zircon	123.9 ± 0.3	290	1.7	**122.8 ± 0.2**	0.92	116.6 ± 2.7	Cretaceous	**Ca. 145 to ca. 66**	Ca. 123 Ma to >66 Ma

Note: *n*—number of detrital grains in youngest peak with overlapping ages within 1σ errors, MSWD—mean square weighted deviation, UNMIX—routine used in Isoplot (Ludwig, 2008) to calculate the mean age and uncertainty for each age group in a population, Y3G—youngest three grains with ages that overlap within 1σ errors. Biostratigraphic ages are based on sparse palynology and macroflora remains (this study) and Walker et al. (2018) time scale (Val—Valanginian; Cen—Cenomanian). Basal lava ages are $^{40}Ar/^{39}Ar$ ages from lavas that underlie the sedimentary strata sampled for biostratigraphy and detrital geochronology. Bold ages indicate those used for interpreted depositional age. Inferred depositional ages are conservative estimates; the upper end of the timing of deposition is based on the broad biostratigraphy constraints and hence is likely much older than the actual cessation and inversion age of these basins. Refer to text for discussion.

Lavas

We report $^{40}Ar/^{39}Ar$ whole-rock ages from five lavas that depositionally underlie the Beaver Lake formation at Beaver Lake and Bonanza Creek (Figs. 5 and 6). Sampled lavas are massive, aphanitic, gray to green-gray units. The lavas yielded $^{40}Ar/^{39}Ar$ ages that range from ca. 122 Ma to ca. 117 Ma (Table 2; Fig. 13). The lava with the youngest age (116.7 ± 0.8 Ma; 16JT07 on Fig. 13) crops out immediately below the lowermost sedimentary strata of the Beaver Lake formation (Fig. 6B). Older ages (ca. 122 Ma to ca. 119 Ma) are from lavas that occur several meters to >100 m below the base of the Beaver Lake formation (Fig. 4). These older ages expand the range of absolute ages reported from the lavas; the oldest previously reported lava age was ca. 117 Ma (Short et al., 2005). The ages of the lavas are not in stratigraphic order, but they overlap in age when analytical uncertainty is considered.

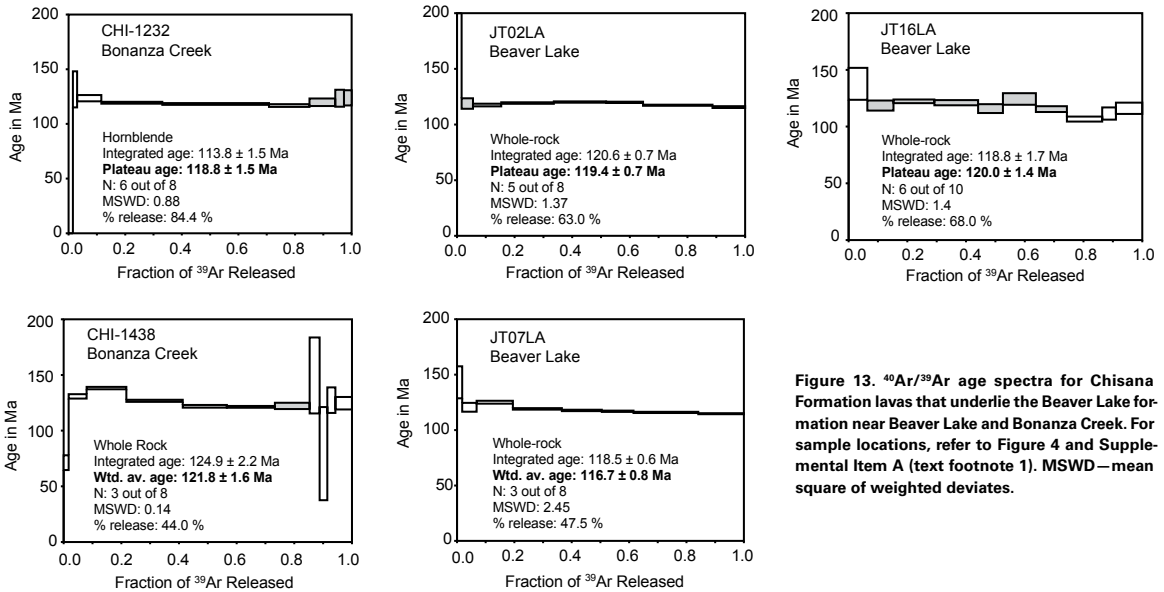

Figure 13. $^{40}Ar/^{39}Ar$ age spectra for Chisana Formation lavas that underlie the Beaver Lake formation near Beaver Lake and Bonanza Creek. For sample locations, refer to Figure 4 and Supplemental Item A (text footnote 1). MSWD—mean square of weighted deviates.

Intrusions

$^{40}Ar/^{39}Ar$ whole-rock ages were obtained from two andesite dikes that crosscut the lower part of the Beaver Lake formation at Beaver Lake. Intrusions sampled are massive, aphanitic, gray-weathering units that crosscut the conglomerate and sandstone, based on our mapping and previous mapping (Richter and Jones, 1973). The intrusions yielded ca. 117 Ma $^{40}Ar/^{39}Ar$ ages (Table 2; Fig. 14).

Totschunda Fault Zone Dike

A homogeneous, pure alkali feldspar separate was prepared from dike sample 01TOT, which was collected from an outcrop near Cooper Pass located ~100 m from the 2002 Denali-Totschunda fault M 7.9 rupture (Fig. 3; Eberhart-Phillips et al., 2003). The sampled dike is an equigranular alkali

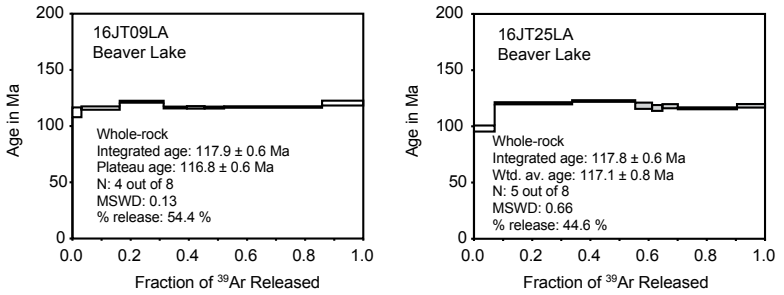

Figure 14. $^{40}Ar/^{39}Ar$ age spectra for intrusions in lowermost sedimentary strata at Beaver Lake. For sample locations, refer to Figure 3 and Supplemental Item A (text footnote 1). MSWD—mean square of weighted deviates.

feldspar syenite, using the classification scheme of Le Maitre et al. (2002). This dike and smaller dikelets were injected into the Totschunda fault zone and cross brittle faults formed within the eastern margin of the Nabesna Pluton (Figs. 3 and 15); thus, it postdates early movement and deformation along the Totschunda fault zone. The integrated age (113.8 ± 1.1 Ma) falls within the uncertainty of the plateau age determination (113.8 ± 1.3 Ma) and the isochron age determination (113.8 ± 1.2 Ma; Table 2; Fig. 15). We prefer the plateau age of 113.8 ± 1.3 Ma because the lower-temperature steps were very imprecise due in part to high atmospheric Ar content, and the plateau age determination has a higher precision than the isochron age determination because of the large uncertainty on the isochron regression to initial $^{40}Ar/^{36}Ar$.

INTERPRETATIONS

Depositional Age of the Beaver Lake Formation

Integrated biostratigraphic and radiometric ages indicate deposition of the Beaver Lake formation during mid-Cretaceous time. Although the collected plant macrofossils do not constrain depositional age, palynomorphs recovered from the Beaver Lake section of the Beaver Lake formation indicate a late Valanginian to early Cenomanian depositional age. Palynomorphs *Cicatricosisporites* sp. and *Osmundacidites wellmani* are long ranging but especially common during Cretaceous time. *Classopollis*? tetrads range from the Sinemurian to Maastrichtian. The maximum age of deposition is based on the presence of *Distaltriangulisporites perplexus*, which is restricted to the late Valanginian to early Campanian (Burden, 1984; Braman, 2001; Payenberg et al., 2002). *Matonisporites* crassiangulatus? ranges from the Hettangian to early Cenomanian (Pocock, 1978; Wingate, 1980). The minimum age of deposition is based on the presence of *Matonisporites* sp., including *Matonisporites crassiangulatus*?. The North American last occurrence of *Matonisporites crassiangulatusis* is late Albian (Singh, 1971; Doyle, 1979; Wingate, 1980). Several other species of *Matonisporites* have their last occurrence in the Cenomanian (May, 1972; May and Traverse, 1973). Thus, we conservatively assign a Cenomanian age for the minimum depositional age.

New geochronologic data support the biostratigraphic data. The youngest lavas that depositionally underlie the Beaver Lake formation yielded ca. 120 to ca. 117 Ma $^{40}Ar/^{39}Ar$ whole-rock ages (Fig. 13), requiring deposition during Aptian or younger time. Intrusions in the lower part of the Beaver Lake formation are ca. 117 Ma, requiring ongoing deposition by this time (Fig. 13). The youngest detrital zircons from the Beaver Lake section are ca. 119 to ca. 117 Ma, indicating deposition during Aptian or younger time (Table 3). Together, the biostratigraphic and radiometric ages indicate deposition of the Beaver Lake section of the Beaver Lake formation initiated ca. 117 Ma but ceased prior to the end of early Cenomanian time (ca. 98 Ma; Table 3).

The depositional age of the Euchre Mountain section is less constrained. No age-diagnostic palynomorphs or plant macrofossils were recovered from the Euchre section of the Beaver Lake formation. The youngest detrital zircons (ca. 123 Ma) and detrital amphiboles (ca. 111 Ma) in the Euchre Mountain section indicate an Aptian–Albian maximum depositional age. Euchre Mountain sandstone layers contain abundant fresh clinopyroxene, a mineral that is abundant in Cretaceous lavas and intrusions throughout the Nutzotin basin, including a pyroxene diorite that crops out <10 km northeast of Euchre Mountain (Richter, 1971; Richter and Jones, 1973); hence, we infer that the Cretaceous detrital zircons and amphiboles were likely derived from these local sources. Given that strata in the Beaver Lake section <20 km away exhibit similar lithologies and plant fossil remains and yield mid-Cretaceous fossil palynomorphs along with dinosaur tracks, we infer a conservative mid- or Late Cretaceous minimum depositional age (ca. 98 Ma) for the Euchre Mountain section. In summary, fossils, detrital ages, and lava ages indicate deposition of the Beaver Lake section was occurring by ca. 117 Ma and ceased by ca. 98 Ma, and deposition of the Euchre Mountain section occurred between ca. 111 Ma and ca. 98 Ma.

Paleoenvironment of the Beaver Lake Formation

Deposition of the Beaver Lake formation occurred in gravelly to sandy channel-bar complexes and associated muddy, vegetated floodplain environments. The sandy-muddy facies association is typical of the deposits of sandy fluvial channel-bar complexes and associated muddy floodplains. Amalgamated units of sandstone and minor conglomerate were deposited as bed load along channel bases and the downstream portions of dunes, bars, and sheets. In contrast, finer-grained lithofacies (Fsm, Fsl, Fsc) are interpreted to represent overbank deposits that formed during and immediately following flooding events (e.g., Slingerland and Smith,

2004). Mud and sand were routed to vegetated floodplain environments from main channels via smaller channels and sheetflows during episodic flood flow. We interpret interbedded fine- to medium-grained sandstones with sharp bases and tabular geometries as crevasse-splay deposits formed during rapid channel avulsion (Allen, 1978). The lack of large-scale inclined strata (lateral accretion structures indicative of bar migration along meanders) and vertical channel stacking patterns suggest an anastomosing river system (Makaske, 2001). Persistently high water tables and frequent disruption by renewed deposition inhibited advanced pedogenesis in floodplain deposits. Sparse laminated mudstones and very rare amorphous kerogen indicate subaqueous suspension settling of mud in flood-basin lakes or ponds, or proximal deltaic environments. Channel banks, bar surfaces, and adjacent floodplains were stabilized by vegetation, judging from preserved roots, upright in situ tree trunks, and abundant conifers and ferns in carbonaceous mudrocks/shales. Episodic forest fires burned this vegetation, as evidenced by abundant charcoal preserved in mudstones. However, the lack of coal beds more than a few centimeters thick indicates little vertical aggradation of organic matter, likely due to the high pace of sediment aggradation and frequent disruption by renewed deposition (Fiorillo et al., 2012).

The gravelly lithofacies association is typical of streamflow processes in gravelly braided stream deposits, including bar/bar-flank and channel-axis deposits (e.g., Bridge and Lunt, 2006). Streamflow and episodic flood flow transported and deposited sand and gravel as bed load along channel bases and the downstream parts of dunes, bars, and sheets. Minor matrix-supported bouldery deposits reflect episodic higher-energy, sediment-laden conditions transitional between hyperconcentrated flow and debris flow. The presence of amalgamated successions of upward-fining, lenticular, <5-m-thick units of sandstone and conglomerate indicates streamflow deposition in relatively shallow, low-sinuosity, braided channels. The limited three-dimensional extent of outcrops prevented detailed characterization of the width and depth of channels and bars and the length and sinuosity of channel bends. The local occurrence of the gravelly association stratigraphically above the finer-grained sandy/muddy association may reflect progradation of higher-gradient, stream-dominated, alluvial-fan environments across lower-gradient, sandy-muddy alluvial plains or distal stream-dominated alluvial fans (e.g., Ridgway and DeCelles, 1993; Trop et al., 2012).

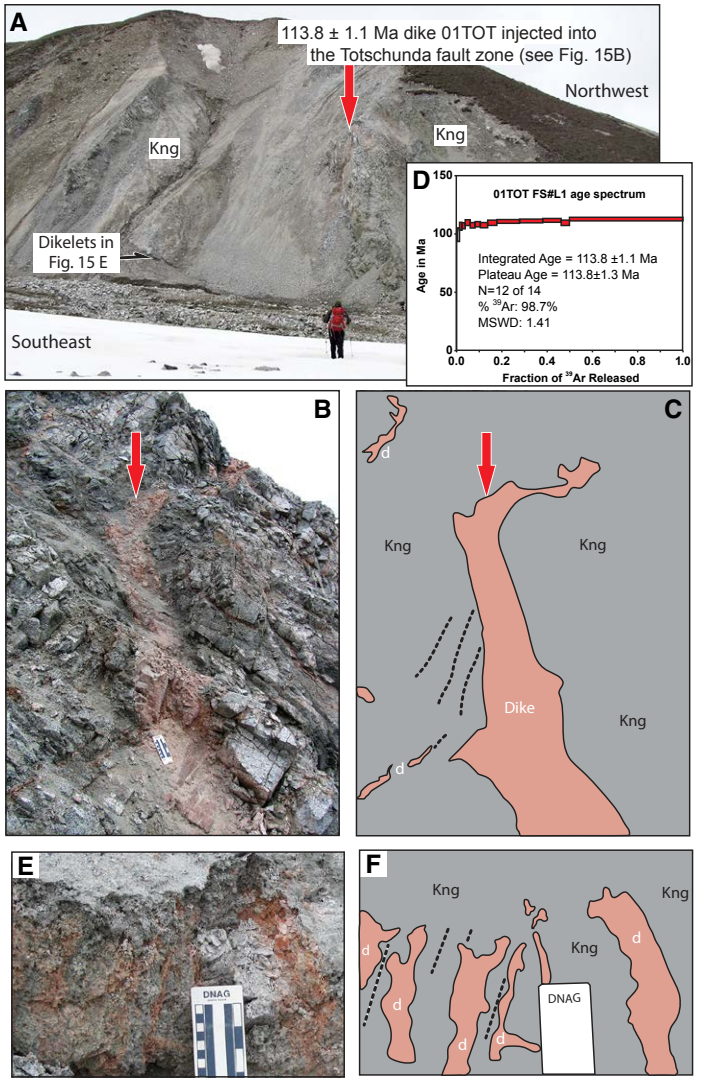

Figure 15. (A) Photographs of pink alkali feldspar syenite dike and dikelets injected into the Totschunda fault zone. Red arrow points to dike surrounded by Nabesna pluton granitoid (Kng). (B) Close-up photograph of dike shown in A. (C) Line drawing of photograph shown in B, where d—dikelets, Kng—granitoid, dashed lines—fault gouge. Refer to Figure 3 for sample location. (D) Age spectrum of potassium feldspars from the dike that yielded a 113.8 ± 1.3 Ma age (this study). MSWD—mean square of weighted deviates. (E) Pink dikelets, <2.5 cm wide, crosscutting Totschunda fault gouge within granitoid. Refer to lower-left part of A for location of dikelets. (F) Line drawing of photograph shown in E, where d—dikelets, Kng—granitoid, dashed lines—fault gouge.

Our new results are well aligned with recent stratigraphic studies from the underlying Chisana volcanic succession that document a progradational up-section transition from subaqueous marine to subaerial processes. At its type section along Bonanza Creek, east of Chisana (Figs. 3 and 4), the lower Chisana Formation consists of basalt

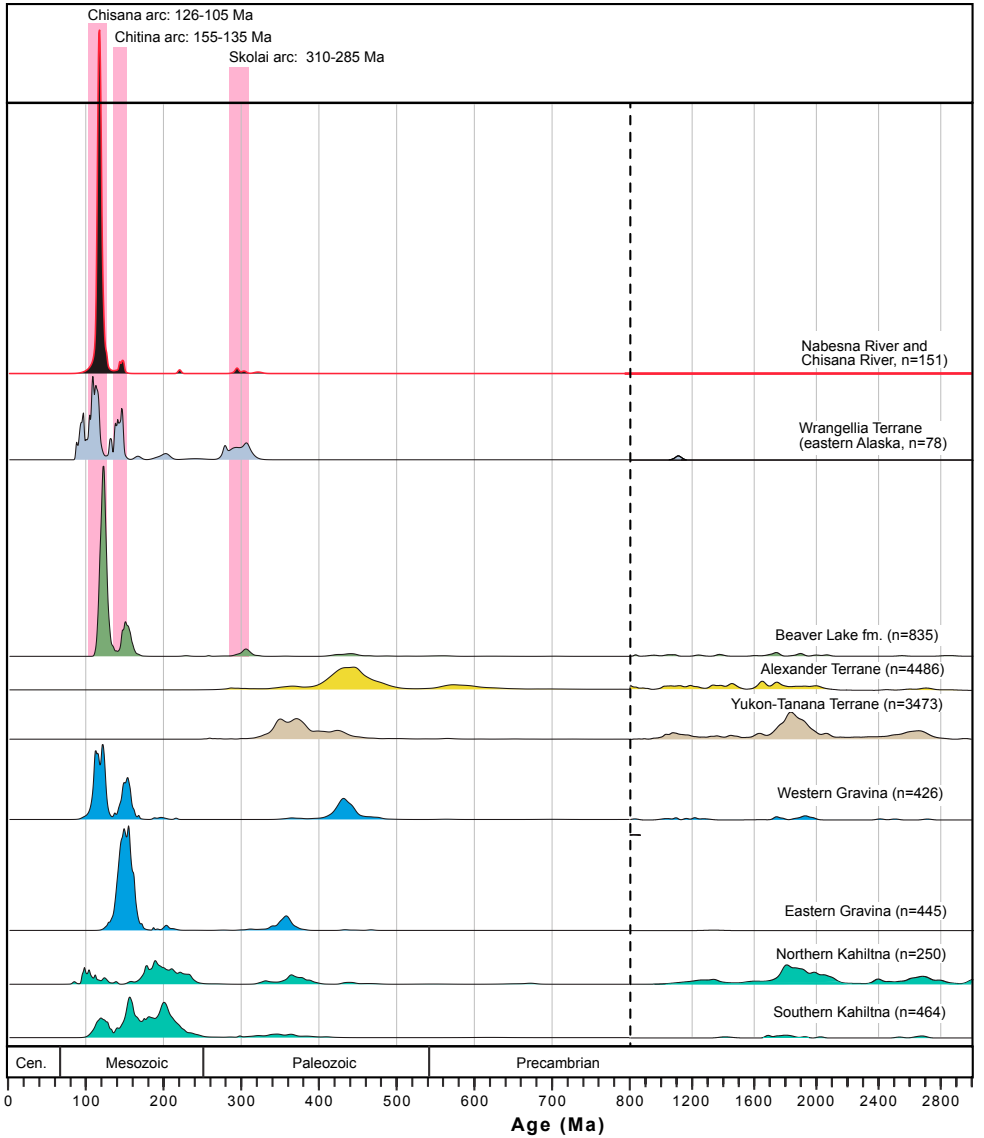

Figure 16. Comparison of U-Pb ages of detrital zircons from the Beaver Lake formation (this study) with reference fields for detrital zircons from modern rivers draining the inboard margin of Wrangellia and Chisana arc rocks (this study), intrusions from Wrangellia and the Alexander terrane in eastern Alaska (Wilson et al., 2015, and references therein), the Alexander terrane in eastern Alaska and SE Alaska (White et al., 2016, and references therein), the Yukon-Tanana terrane in SE and eastern Alaska (Pecha et al., 2016, and references therein), the Kahiltna assemblage (Hampton et al., 2010), and the Gravina assemblage (Yokelson et al., 2015). Pink vertical bars mark arc flare-ups within Wrangellia in south-central Alaska (Wilson et al., 2015, and references therein; Beranek et al., 2014; Graham et al., 2016). Age-distribution curves have 10× vertical exaggeration for ages older than 800 Ma. Other parameters of this plot are adapted from Figure 12. Cen—Cenozoic.

to andesite lavas, with local pillows, mudstone, and volcaniclastic conglomerates with marine fossils, breccia, and block-and-ash deposits that record effusive eruptions, lahars, and pyroclastic eruptions, mainly under subaqueous marine conditions (Sandy and Blodgett, 1996; Short et al., 2005; Manselle et al., 2018). The uppermost part of the volcanic stratigraphic, and isolated outcrops near Nabesna, consist of oxidized, autobrecciated tops/bases and volcaniclastic conglomerates interpreted as the deposits of subaerial effusive eruptions (Manselle et al., 2018).

Our new sedimentologic and age data provide new constraints on the age of dinosaur footprints reported previously from the Beaver Lake formation. Fiorillo et al. (2012) reported footprints from two types of dinosaurs, theropods and ornithopods (cf. hadrosaurids). Our sedimentological data sets confirm previous interpretations by Fiorillo et al. (2012) that the dinosaurs inhabited an environment characterized by variable fluvial subenvironments stabilized by abundant vegetation prone to fire and channel migration. New age data presented herein indicate that the previously documented dinosaur footprints are ca. 117–98 Ma (late Aptian to early Cenomanian). Most Alaskan dinosaurs are reported from Campanian–Maastrichtian (ca. 84–66 Ma) strata in south-central or northern Alaska, although some fossils occur in Late Jurassic and Early Cretaceous strata in south-central Alaska (Fiorillo, 2006).

Provenance of the Beaver Lake Formation

The dominance of volcanic and plutonic clasts in Beaver Lake formation conglomerate and the abundance of unstable pyroxene, amphibole, and volcanic-lithic grains in sandstone suggest detritus was transported relatively short distances from local igneous source terranes. The most likely source candidates are Jurassic–Cretaceous plutons and volcanic rocks that crop out within Wrangellia and the Nutzotin basin. The dominant group of detrital zircon ages (age peak of ca. 122 Ma on Fig. 16) overlaps the age range of Chisana arc plutons and volcanic rocks that crop out near the Beaver Lake formation along the inboard margin

of Wrangellia (Kc and Kg on Fig. 3; Richter et al., 1975; Short et al., 2005; Snyder and Hart, 2007; this study). Recently reported U-Pb zircon ages reported from the Nabesna and Klein Creek Plutons are 126–113 Ma (Fig. 3; Graham et al., 2016). Our new detrital zircon ages from modern rivers that drain Chisana arc igneous rocks in the Nutzotin basin yielded similar detrital zircon age peaks (118 Ma age peaks for both the Nabesna and Chisana Rivers on Figs. 3 and 12). The Cretaceous lavas and plutons that crop out around the Nutzotin basin are lithologically similar to mafic/intermediate and granitoid clasts that dominate Beaver Lake formation conglomerates (Chisana arc; Richter, 1976; Manselle et al., 2018). Late Early Cretaceous igneous rocks presently exposed on the opposite side of the Denali fault in Canada may have also contributed early Late Cretaceous igneous detritus; at least ~370 km of post–Early Cretaceous dextral slip is inferred along the Denali fault since deposition (Fig. 3; Lowey, 1998). Subordinate ca. 151 Ma and ca. 306 Ma detrital zircon age peaks (Fig. 16) match ages reported from intrusions in Wrangellia and Alexander terrane (Chitina and Skolai arcs; Grantz et al., 1966; Trop et al., 2002; MacKevett, 1978; Plafker et al., 1989; Beranek et al., 2014) and detrital age peaks in modern rivers draining Wrangellia (Bliss et al., 2017).

Minor Paleozoic to Proterozoic detrital zircon age peaks in Beaver Lake strata (440, 487, 560, 1051, 1079, 1372, 1737, and 1890 Ma) are broadly similar to zircon age populations reported from the Alexander terrane to the south and the Yukon-Tanana terrane to the north. Paleozoic–Proterozoic rocks of the Alexander terrane in eastern Alaska and southeastern Alaska have well-defined age peaks ca. 490–410 Ma and 610–520 Ma, as well as minor populations spanning 2300–900 Ma (Beranek et al., 2013; Tochilin et al., 2014; White et al., 2016). Detrital zircon U-Pb ages from Paleozoic metasedimentary strata of the Yukon-Tanana terrane in eastern Alaska, Yukon Territory, and southeastern Alaska yield a broad distribution of ages from 900 to 2400 Ma, including a well-defined peak between 2000 and 1700 Ma (Nelson and Gehrels, 2007; Pecha et al., 2016) that occurs in the sampled Beaver Lake sandstones. However, Beaver Lake formation samples lack the 380–340 Ma age population reported from crystalline rocks from the Yukon-Tanana terrane of eastern Alaska and Yukon Territory (Aleinikoff et al., 1981, 1986; Aleinikoff et al., 1984; Dusel-Bacon et al., 2006; Dusel-Bacon and Williams, 2009; Day et al., 2014).

In summary, sandstone and conglomerate clast compositions, and zircon U-Pb and amphibole $^{40}Ar/^{39}Ar$ detrital geochronology indicate that the provenance of Beaver Lake strata was chiefly the Cretaceous Chisana magmatic arc igneous rocks along the inboard margin of Wrangellia. Subordinate detrital age peaks indicate minor sediment contributions from Late Jurassic, Pennsylvanian–Permian, Ordovician–Silurian, and Proterozoic sources in Wrangellia and the adjacent Alexander terrane (Fig. 1). Sparse Proterozoic U-Pb detrital zircon ages presented here are consistent with erosion of the Alexander terrane and/or the Yukon-Tanana terrane to the north. Beaver Lake formation sandstones yielded 1.8 Ga zircons that are widespread in the Yukon-Tanana terrane and make up minor components of the Alexander terrane. The ca. 360–340 Ma zircon ages that also typify the Yukon-Tanana terrane are not evident in the sampled Beaver Lake formation strata. Thus, additional detrital geochronologic studies from the Beaver Lake formation are warranted to evaluate potential sediment contributions from inboard terranes such as the Yukon-Tanana terrane.

Initiation of the Totschunda Fault System

The integrated age and/or plateau age for unaltered potassium feldspar samples can reflect the complete cooling history of a sample that cools quickly from ~350 °C to ~150 °C (e.g., Lovera et al., 2002; Benowitz et al., 2011, 2012, 2014; Riccio et al., 2014). K-feldspar thermochronology (KFAT) of sample 01TOT has a slightly down-stepping age spectrum that may reflect rapid cooling over several million years (KFATmax Tc ~350°C = 115.2 ± 1.6 Ma; KFATmin Tc ~150°C = 108.9 ± 3.4 Ma), or this age spectrum may be an artifact of the large uncertainty on each individual step or subsequent minor hydrothermal effects. Given the consistent Ca/Ka ratio of < 0.5 for each step release and lack of obvious sericite in the dike sample, we infer that alteration of the dike after emplacement was not significant factor in Ar retention or Ar release patterns during the incremental step-heating experiment. We infer that the plateau age determination best reflects the magmatic age of this sample, although the dike likely did not cool fully at 113.8 Ma.

The dike was emplaced into a slightly an older granitoid, the Nabesna Pluton (Fig. 3). The Nabesna Pluton yielded U-Pb zircon ages of 118.2 ± 0.6 Ma, 117.6 ± 1.0 Ma, and 113 ± 0.5 Ma (Fig. 3; Graham et al., 2016). We infer a ca. 118 Ma age for the main phase of magmatism in the pluton, given the bedrock ages together with a ca. 118 Ma age peak in detrital zircon ages from rivers draining the pluton (Fig. 12).

The 113.8 ± 1.3 Ma dike, 01TOT, crosses brittle faulting in the Nabesna Pluton and intrudes preexisting Totschunda fault gouge (Fig. 15). The 30-cm-thick dike cooled very rapidly and hence was most likely injected into shallow crust, consistent with field observations that the dike was intruded into a preexisting fault zone, based on the presence of brittle faulting and gouge.

This type of isolated syntectonic diking is common in strike-slip fault zones (Leloup et al., 2011; Betka et al., 2017). Tens of meters away from the 01TOT dike outcrop, there is a region of pure fault gouge with injected dikelets that appear to have similar compositions to sample 01TOT, but we did not date nor sample these dikelets. These dikelets and the 01TOT dike are the only known dikes intruding the Nabesna Pluton in the sampled area. Hence, the 114 Ma dike we dated and the observed neighboring dikelets injected into fault gouge imply the Totschunda fault was active by this time and creating accommodation space for the dike, likely via transtensional deformation.

Regional Paleogeographic and Tectonic Implications

The Beaver Lake formation is an important sedimentary succession in the northwestern Cordillera because it provides a rare stratigraphic

record of the transition from marine to nonmarine depositional conditions along the inboard margin of Wrangellia during Cretaceous time. New data sets presented here from the Beaver Lake formation demonstrate that the formerly marine Nutzotin basin that separated Wrangellia from inboard terranes was subaerially exposed by ca. 117 Ma. Environments evolved from steep submarine slopes/fans characterized by mass flows to fluvial environments bordered by floodplains and wetlands with dinosaurs and diverse vegetation. Detritus was eroded chiefly from late Early Cretaceous arc-related plutons and volcanic centers within Wrangellia. Minor Paleozoic and Proterozoic age peaks reflect minor sediment derivation from the Alexander terrane and possibly the former continental margin (i.e., Yukon-Tanana terrane). Fluvial deposition recorded by the Beaver Lake formation slightly preceded deposition of lithologically similar fluvial strata deposited ca. 113–94 Ma along the inboard margin of Wrangellia in the Talkeetna Mountains, ~350 km west of the Beaver Lake formation outcrops (Figs. 2 and 17; Hampton et al., 2007, 2017). The Caribou Pass Formation fluvial strata yielded detrital zircon populations that reflect sediment contributions from both the Insular and Yukon-Tanana terranes (Fig. 17).

Similarly, provenance data from Gravina belt strata in southeastern Alaska show that broadly coeval strata were shed from the Alexander terrane and Jurassic–Cretaceous volcanic and plutonic rocks that intrude or overlie the Alexander terrane as well as inboard terranes (Berg et al., 1972; Rubin and Saleeby, 1991, 1992; McClelland et al., 1992; Cohen and Lundberg, 1993; Cohen et al., 1995; Kapp and Gehrels, 1998; Yokelson et al., 2015). Slightly younger Aptian–Albian strata in the lower Matanuska Formation along the outboard margin of the Peninsular terrane in south-central Alaska yielded provenance data that indicate erosion of both the Insular and Yukon-Tanana terranes (Fig. 17; Reid et al., 2018). Sedimentologic studies indicate that the preserved strata accumulated in open-marine environments, but nonmarine strata crop out locally, including Albian coal-bearing fluvial strata (Fig. 17; Grantz, 1964; Trop et al., 2002; Stevens Goddard et al., 2018). Albian and younger forearc strata overlie older strata along a basinwide angular unconformity (Grantz, 1964; MacKevett, 1978) that is interpreted to reflect regional shortening associated with accretion/suturing of the Insular terranes against inboard terranes during Early Cretaceous time (Trop et al., 2002, 2005; Trop, 2008; Stevens Goddard et al., 2018).

Detrital zircon age distributions from the Beaver Lake formation support the timing for the same magmatic pulses and lulls as reported previously along the northern Cordillera orogen (Gehrels et al., 2009). The detrital ages indicate high-flux magmatic periods during Late Jurassic and late Early Cretaceous time, separated by an Early Cretaceous ca. 140–130 Ma magmatic lull that is similar to the plutonic record for the Insular terranes (Fig. 16; Rioux et al., 2007; Snyder and Hart, 2007) and detrital zircon age populations from the Gravina belt (Yokelson et al., 2015), Kahiltna assemblage (Hampton et al., 2010), Jurassic–Cretaceous strata in the Matanuska Valley–Talkeetna Mountains basin (Stevens Goddard et al., 2018; Reid et al., 2018), and accretionary prism strata in the Chugach terrane (Haeussler et al., 2006; Amato et al., 2013; Garver and Davidson, 2015). The scarcity of ca. 140–125 Ma ages may reflect a magmatic lull in response to an oblique sinistral component of plate convergence (Engebretson et al., 1985; Gehrels et al., 2009). Faults along the margin of the Insular terranes in southeastern Alaska and western British Columbia record sinistral displacements at ca. 110 Ma (Fig. 17; Chardon et al., 1999; Chardon, 2003; Butler et al., 2006; Mahoney et al., 2009), but motion may have commenced earlier in Cretaceous time. Direct evidence for Early Cretaceous sinistral displacements in south-central and eastern Alaska has not been reported.

During mid-Cretaceous time, the Jurassic–Cretaceous basinal assemblages between the Insular terranes and inboard terranes were shortened and uplifted by a regionally extensive thrust system documented for >2000 km along the northern Cordillera margin (Fig. 17; Rubin et al., 1990; Evenchick et al., 2007; Rusmore and Woodsworth, 1991, 1994; Ridgway et al., 2002). Deformation was accommodated by shear zones, high-angle faults, and inboard-dipping (east- to northeast-dipping) thrust faults that regionally juxtaposed marine strata against the Insular terranes (Rubin and Saleeby, 1991; Davidson et al., 1992; Manuszak et al., 2007). In the Nutzotin basin, Cretaceous marine sedimentary strata were folded and thrust southward along the north-dipping Lost Creek décollement before emplacement of ca. 117 ± 3.5 Ma intrusions (Figs. 3, 17, and 18; Richter et al., 1975; Manuszak et al., 2007). The Totschunda fault also initiated within the Nutzotin basin during this time interval, as shown by the new data presented herein. A dike that intruded into and crosscut brittle deformed rock of the Totschunda fault zone yielded a 113.8 ± 1.1 Ma $^{40}Ar/^{39}Ar$ age (this study; Figs. 15, 17, and 18). Geophysical constraints indicate the >200-km-long Totschunda fault is a major structure that separates crustal blocks of differing rheology, as indicated by substantial variations in seismic velocities across the fault (Allam et al., 2017). Allam et al. (2017) inferred that the Moho is displaced across the fault, judging from the velocities. Thermochronology results indicate the fault experienced episodes of vertical tectonic activity at ca. 90 Ma, ca. 80 Ma, ca. 55 Ma, and ca. 25 Ma (Milde, 2014). The neighboring Duke River fault, which splays from the southern terminus of the Totschunda fault (Fig. 1), separates the Alexander terrane and Wrangellia and was active by ca. 105 Ma, according to $^{40}Ar/^{39}Ar$ dates from muscovite that grew during faulting or was reset by motion along the Duke River fault (Cobbett et al., 2016). The initiation and activity along the Lost Creek décollement, the Totschunda fault, and the Duke River fault during Aptian–Albian time imply that this was a period of regional deformation within the Insular terranes. These structures were likely reactivated during dextral transpression of uncertain magnitude during latest Cretaceous to Paleocene time (Andronicos et al., 1999; McClelland and Mattinson, 2000; Stamatakos et al., 2001). Recent seismicity and surface ruptures demonstrate that the Totschunda fault remains active (Eberhart-Phillips et al., 2003).

Broad open folds with northwest-southeast–striking axes deform the Beaver Lake formation strata, as well as underlying Late Jurassic–Early Cretaceous marine sedimentary and volcanic strata of the Nutzotin Mountains sequence and

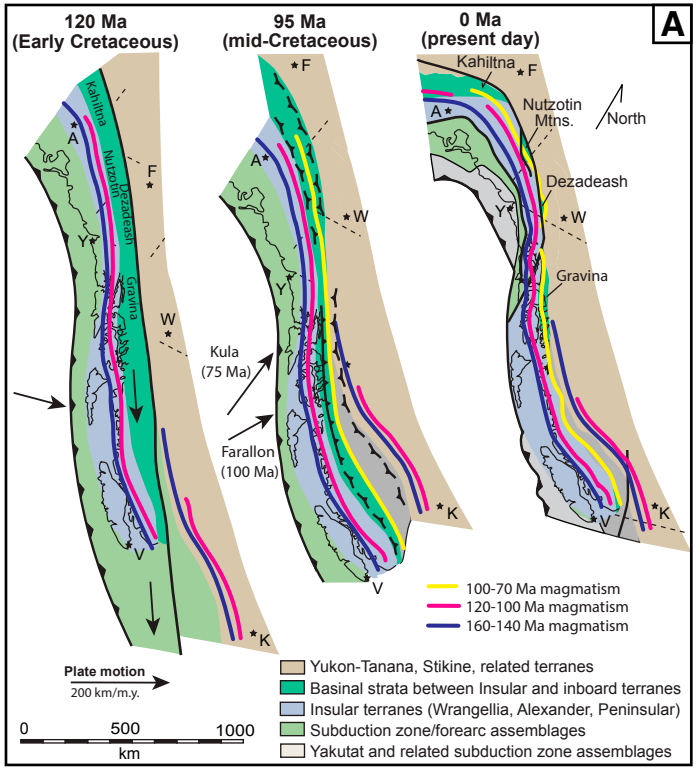

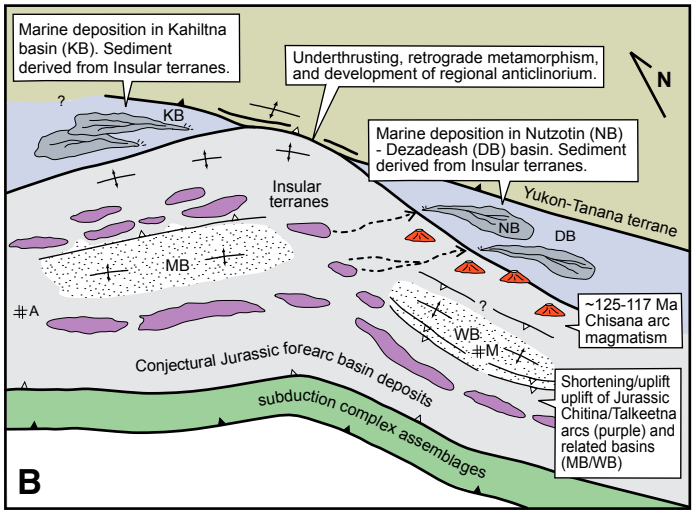

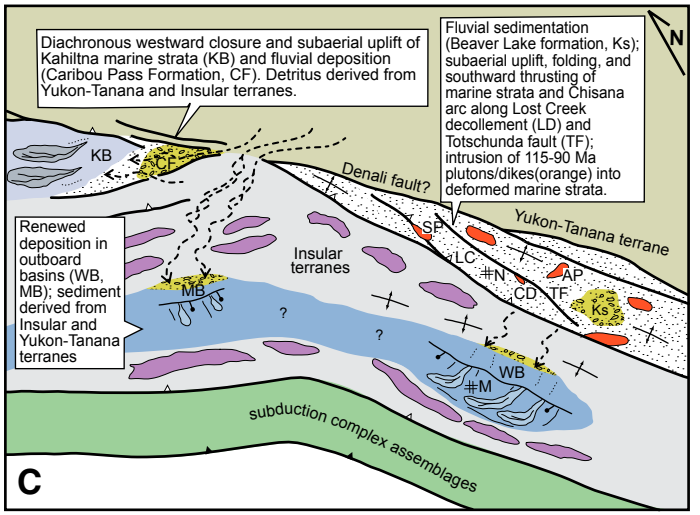

Figure 17. (A) Schematic tectonic model adapted from Gehrels et al. (2009) showing Cretaceous evolution of northern Cordillera margin, including changes in plate motion (from Engebretson et al., 1985), closure of marine basins along inboard margin of Insular terranes, shifts in arc magmatism, and lateral shuffling of terranes along regional strike-slip faults. See text and Gehrels et al. (2009) for discussion. Modern towns for reference: A—Anchorage, F—Fairbanks, K—Kelowna, V—Vancouver, W—Whitehorse, Y—Yakutat. (B, C) Schematic maps showing closure, subaerial emergence, and deformation of the formerly marine basins separating the Insular terranes from inboard terranes in eastern and south-central Alaska. Abbreviations: AP—ca. 105 Antler Creek pluton, CD—ca. 114 Ma Cooper Pass dike in Totschunda fault, CF—Caribou Pass Formation, DB—Dezadeash basin, KB—Kahiltna basin, Ks—ca. 117 Ma Cretaceous fluvial strata (Beaver Lake formation), LC—Lost Creek décollement (thrust fault), MB—Matanuska basin, NB—Nutzotin basin, SP—ca. 114 Ma Suslota Pass pluton, TF—Totschunda fault, WB—Wrangell Mountains basin, YT—Yukon Tanana terrane. Modern towns for reference: #A—Anchorage, #N—Nabesna, #M—McCarthy. Figure is modified from Trop and Ridgway (2007).

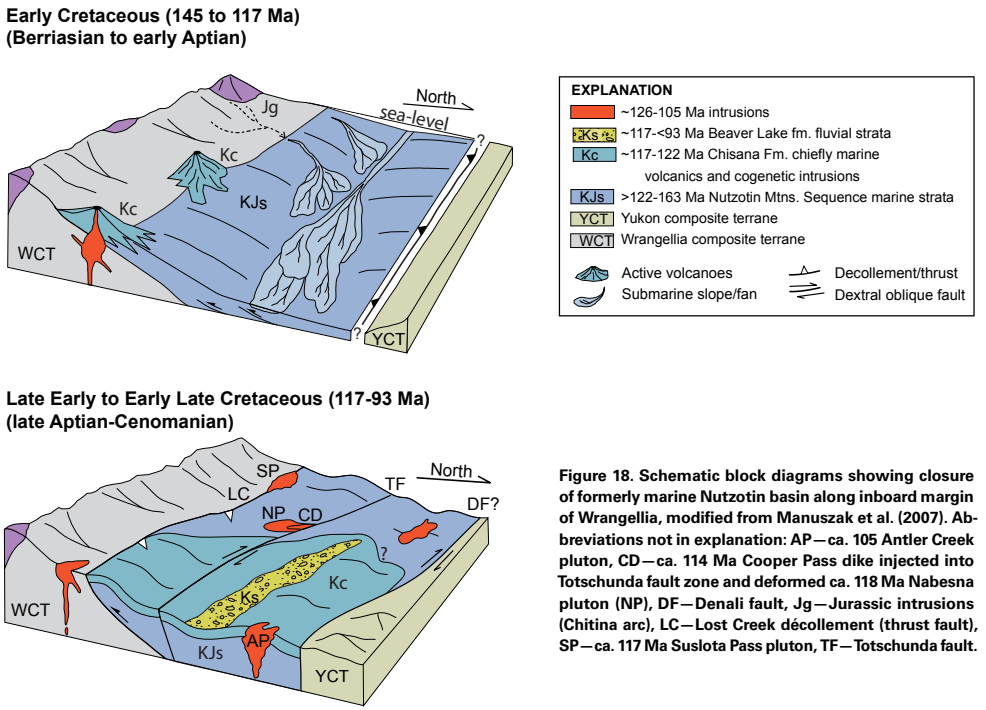

Figure 18. Schematic block diagrams showing closure of formerly marine Nutzotin basin along inboard margin of Wrangellia, modified from Manuszak et al. (2007). Abbreviations not in explanation: AP—ca. 105 Antler Creek pluton, CD—ca. 114 Ma Cooper Pass dike injected into Totschunda fault zone and deformed ca. 118 Ma Nabesna pluton (NP), DF—Denali fault, Jg—Jurassic intrusions (Chitina arc), LC—Lost Creek décollement (thrust fault), SP—ca. 117 Ma Suslota Pass pluton, TF—Totschunda fault.

Chisana Formation (Figs. 3 and 4; Richter, 1976; Manuszak et al., 2007). The orientations of the fold axes are consistent with postdepositional transpressive shortening in a zone of right-lateral shear between the Totschunda and Denali faults (note strain ellipses on Fig. 3). Evidence for syndepositional displacement along the faults has not been demonstrated in the Jurassic–Cretaceous strata (Nutzotin Mountains sequence, Chisana Formation, Beaver Lake formation); there is no evidence of localized thickening of strata across faults, and intraformational unconformities are not evident. Alternatively, shortening may have been unrelated to strike-slip tectonics and initiated mainly by mid-Cretaceous accretion/collision of the Insular terrane. Unfortunately, the timing and kinematics of faults that cut the Nutzotin basin fill are not well established. Understanding the complete history of basin development will require geochronologic studies together with field studies of the faults and their relationships with Cretaceous volcanic and sedimentary rocks.

The presence of ca. 190 Ma apatite fission-track ages (Milde, 2014) and the relatively gently deformed Cretaceous sedimentary packages along the east side of the Totschunda fault imply minimum contractional deformation across this structure since inception. Strike-slip faults with significant displacement histories (>100 km) are known to have significant exhumation-deformation histories (e.g., Alpine fault of southern New Zealand—Batt et al., 2004; San Andreas fault—Spotila et al., 2007; Denali fault—Benowitz et al., 2014; Fitzgerald et al., 2014; Burkett et al., 2016). Given this context and the presence of Jurassic–Cretaceous sedimentary and volcanic strata (Nutzotin Mountains sequence and Chisana Formation) and Oligocene–present volcanic-plutonic rocks (Wrangell arc; Brueseke et al., 2019) on both sides of the Totschunda fault (Fig. 3; Richter, 1976; Brueseke et al., 2019), we infer the fault has not experienced large magnitudes (i.e., hundreds of kilometers) of strike-slip motion since inception during Cretaceous time.

Existing tectonic models broadly agree on closure of the Gravina, Nutzotin-Dezadeash, and Kahiltna marine basins but differ in interpretations of the original sizes of the marine basins and the geometry of the subduction zones that bounded them. One family of models, mainly based on geologic and paleomagnetic data, shares a common interpretation of east-/northeast-dipping subduction zones during Jurassic–Cretaceous time. Variants include the inferred timing of collision with the North American margin (Hults et al., 2013) and the role of back-arc opening and closure (Lowey, 2018). Nonetheless, our preferred interpretation is that the Kahiltna, Nutzotin, and Gravina marine depocenters closed along a pair of east-dipping subduction zones, one along the eastern (inboard) margin of the Insular terranes and one along the western (outboard) margin of the Insular terranes (Fig. 17; Trop and Ridgway, 2007, their figure 4).

A second group of models, supported chiefly by tomographic images of the mantle beneath eastern North America, suggests closure by a west-dipping subduction zone along the eastern edge of the Insular terrane that was active into mid-Cretaceous time in the northern Cordillera and latest Cretaceous in the south (Sigloch and Mihalynuk, 2013, 2017). According to Sigloch and Mihalynuk (2013, 2017), the Nutzotin basin was part of an extensive ocean basin that was consumed by west-dipping subduction along the inboard margin of the Insular terrane between ca. 140 Ma and ca. 110 Ma. Their evidence consists of near-vertical zones in the mantle that have higher-than-average seismic velocities and extend from ~800 to ~2000 km depth. However, that scenario is inconsistent with geologic data, which are interpreted to document sedimentary linkages among the Kahiltna, Nutzotin, and Gravina basins and the inboard margins of the Insular terranes from Late Jurassic (ca. 160 Ma) through mid-Cretaceous (ca. 110 Ma) time (Hampton et al., 2010; Manuszak et al., 2007; Yokelson et al., 2015; this study), coeval with arc magmatism within the Insular terranes and subduction complex deposits that

reflect east-dipping subduction beneath the Insular terranes (Plafker et al., 1994; Amato et al., 2013). Pavlis et al. (2019) discussed additional geologic data that argue against the west-dipping subduction model. Following Monger (2014), Yokelson et al. (2015), and Pavlis et al. (2019), we conclude that a west-dipping subduction zone along the inboard margin of the Insular terranes between ca. 140 Ma and ca. 110 Ma is an unlikely explanation of the tomographic results presented by Sigloch and Mihalynuk (2013, 2017).

In summary, our new sedimentological data and recently reported dinosaur footprints in the Beaver Lake formation (Fiorillo et al., 2012) indicate subaerial exposure of the Nutzotin basin and connections with both the Insular terranes and inboard terranes along the former continental margin by ca. 117 Ma (Figs. 17 and 18). We infer that the subaerial deposition reflects closure of the formerly marine ocean basin that separated the Insular terrane from inboard terranes. Short-term sea-level regressions may have contributed to the shift from relatively deep-marine submarine slope/fan environments to terrestrial deposition; however, relatively high and stable sea levels characterized late Aptian–Albian time (Haq, 2014). Higher-resolution depositional age data are needed to fully evaluate the roles of eustasy and tectonics on relative sea level. The shift to subaerial deposition was coeval with regional crustal shortening. South of the Nutzotin basin in the Wrangell Mountains, Upper Jurassic and older sedimentary strata of Wrangellia are deformed by regional folds and thrust faults and overlain by Albian sedimentary strata along an angular unconformity (Trop et al., 2002). Jurassic–Early Cretaceous strata of the Nutzotin Mountains sequence marine strata were thrust over Wrangellia along a northeast-dipping décollement (Lost Creek décollement on Fig. 3) and intruded by an undeformed pluton that yielded a 117 ± 3.5 Ma K-Ar age (Richter et al., 1975; Manuszak et al., 2007). The suture zone evolved from a relatively deep-marine basin along the inboard margin of Wrangellia to a broad zone of crustal thickening through the addition of mid-Cretaceous intrusions and mid-Cretaceous deformation along regional faults, including the Lost Creek décollement, the Totschunda fault, and the Duke River fault (Figs. 17 and 18). The suture zone has been reactivated during Late Cretaceous–Cenozoic plate convergence, as evidenced by recent seismicity along the Denali and Totschunda faults.

SUMMARY AND CONCLUSIONS

Sedimentary, volcanic, and fault zone rocks exposed in the Nutzotin basin record important interactions between the Wrangellia-Alexander terrane and the North American margin during Late Jurassic through mid-Cretaceous time. This study presents new sedimentologic, paleontologic, and geochronologic data from previously unnamed strata that record subaerial emergence of the formerly marine basin that separated the Wrangellia-Alexander terrane from the continental margin. In this report, the previously unnamed strata are referred to as the Beaver Lake formation. Lithofacies and paleobotanical data from the Beaver Lake formation document the depositional processes and environments. Volcanic-lithic sandstone, conglomerate, carbonaceous mudrock, and sparse coal indicate streamflow deposition in channel-bar complexes and vegetated floodplains with poorly drained wetlands. The terrestrial nature of recovered kerogen and palynomorph assemblages and well-preserved terrestrial plant macrofossils support deposition in humid fluvial environments with forested floodplains and wetlands. U-Pb and $^{40}Ar/^{39}Ar$ ages of detrital zircons and amphiboles and conglomerate compositional data constrain the timing of nonmarine deposition and evaluate possible provenance ties with adjacent terranes. The $^{40}Ar/^{39}Ar$ ages from lavas underlying the Beaver Lake formation provide additional constraints on the timing of fluvial deposition. Nonmarine deposition commenced by ca. 117 Ma, as evidenced by the youngest detrital ages, age-diagnostic palynomorphs, ages of lavas that underlie the fluvial strata, and ages of intrusions into the fluvial strata. Sediment was eroded chiefly from local volcanic-plutonic arc source terranes, judging by the presence of unstable mineral grains in sandstone, mainly pyroxene and amphibole, the dominance of volcanic and plutonic clasts in conglomerate, and the dominance of late Early Cretaceous detrital zircon and hornblende age peaks, which are similar to ages reported from the adjacent Chisana arc along the inboard margin of Alexander-Wrangellia terrane. Minor Late Jurassic and Pennsylvanian–Permian detrital zircon age peaks overlap with ages previously reported from older crystalline rocks from the Alexander-Wrangellia terrane. Minor early Paleozoic and Proterozoic detrital zircon age populations overlap with ages reported from the Alexander terrane to the south and the Yukon-Tanana terrane to the north. The suture-bounding Totschunda fault was active by at least ca. 114 Ma, syntectonic with deposition of the Beaver Lake formation at Beaver Lake.

We propose a model in which the Insular terranes were sutured against inboard terranes during late Mesozoic time (Figs. 17 and 18). Our preferred scenario is as follows:

(1) Late Jurassic–Early Cretaceous marine deposition and arc magmatism occurred along the inboard margin of the Wrangellia-Alexander terrane in the Nutzotin, Dezadeash, Kahiltna, and Gravina basins (Monger et al., 1994; Hampton et al., 2010; Lowey, 2011; Hults et al., 2013; Yokelson et al., 2015). Inboard basins presently exposed in southeastern Alaska and Canada formed following suturing of the Insular terranes against inboard terranes by mid-Jurassic time (Monger et al., 1994; Gehrels et al., 2009; Yokelson et al., 2015), whereas inboard basins presently exposed in south-central and eastern Alaska record suturing during Late Jurassic to late Early Cretaceous time (Ridgway et al., 2002; Hampton et al., 2010; Trop et al., 2002, 2005; this study). Subduction complex and forearc-basin strata exposed along the outboard (southeastern) margin of the Insular terranes record sediment flux chiefly from Late Jurassic–Early Cretaceous southwest-facing volcanic arcs within the Insular terranes (Amato et al., 2013; Stevens Goddard et al., 2018).

(2) Formerly marine basins exposed along the inboard margin of the Wrangellia-Alexander terrane in south-central Alaska became

subaerially exposed during Aptian–Albian time, based on sedimentologic and paleontologic data sets from the Kahiltna and Nutzotin basins (Hampton et al., 2017, 2017; Fiorillo et al., 2012; this study). We attribute this change to accretion-related crustal shortening along the inboard margin of the Insular terrane. The transition from marine to terrestrial deposition in sedimentary basins throughout much of the Wrangellia-Alexander terrane was coeval with regional crustal shortening and unconformity development within the Wrangellia-Alexander terrane and the appearance of continental-margin–affinity detrital zircons (Hampton et al., 2007, 2017; Trop et al., 2002; Reid et al., 2018). Terrestrial deposition commenced in eastern Alaska during Aptian time (this study) and in central Alaska during Albian–Cenomanian time (Hampton et al., 2007, 2017).

(3) Late Cretaceous–Cenozoic plate convergence and dextral transpression along strike-slip faults prompted shortening and lateral shuffling of the Jurassic–Cretaceous basins (Kahiltna, Nutzotin, Dezadeash, and Gravina basins) and magmatic belts along the inboard margin of the Insular terrane (Gehrels et al., 2009; Benowitz et al., 2011; Waldien et al., 2018). At least 370 km of dextral strike-slip motion along the Denali fault displaced previously linked marine basin deposits of the Nutzotin and Dezadeash basins (Lowey, 1998). The Totschunda and Duke River faults, which originated by 114–105 Ma (Cobett et al., 2016; this study), displaced the Jurassic–Cretaceous Nutzotin basin.

(4) Collision and flat-slab subduction of the Yakutat terrane prompted regional deformation, exhumation, and arc magmatism in south-central and eastern Alaska during Cenozoic time (Finzel et al., 2011). During this phase, arc magmatism and intra-arc strike-slip faulting and alluvia-fluvial sedimentation overprinted the Nutzotin basin starting ca. 30 Ma (Trop et al., 2012; Brueseke et al., 2019).

ACKNOWLEDGMENTS

This research was made possible in part by funding from the National Science Foundation (NSF) to Brueseke (EAR-1450689), Benowitz and Layer (EAR-1450730), and Trop (EAR-1450687). We thank everyone at Devil's Mountain Lodge for logistical support; staff of the National Park Service Alaska Region (NPS) and Wrangell–St. Elias National Park and Preserve for assistance; Arizona LaserChron Center for assistance with geochronological analyses; University of Alaska–Fairbanks student K. Davis; Kansas State University students B. Morter and S. Berkelhammer for assistance in the field; Bucknell University student B. Moretti for assistance with geographic information system mapping and geochronologic analyses; and G. Graham for sharing geochronologic data and sample locations. G. Andrews, J. Toro, S. Israel, and an anonymous reviewer provided feedback on an earlier version of this manuscript.

REFERENCES CITED

Aleinikoff, J.N., Dusel-Bacon, C., and Foster, H.L., 1981, Geochronologic Studies in the Yukon-Tanana Upland, East-Central Alaska, *in* Accomplishments during 1979: U.S. Geological Survey Circular 823-B, p. B34–B37.

Aleinikoff, J.N., Foster, H.L., Nokleberg, W.J., and Dusel-Bacon, C., 1984, Isotopic Evidence from Detrital Zircons for Early Proterozoic Crustal Materials, East-Central Alaska, *in* Accomplishments during 1981: U.S. Geological Survey Circular 868, p. 43–45.

Aleinikoff, J.N., Dusel-Bacon, C., and Foster, H.L., 1986, Geochronology of augen gneiss and related rocks, Yukon-Tanana terrane, east-central Alaska: Geological Society of America Bulletin, v. 97, p. 626–637, https://doi.org/10.1130/0016-7606(1986)97<626:GOAGAR>2.0.CO;2.

Allam, A.A., Schulte-Pelkum, V., Ben-Zion, Y., Tape, C., Ruppert, N., and Ross, Z.E., 2017, Ten kilometer vertical Moho offset and shallow velocity contrast along the Denali fault zone from double-difference tomography, receiver functions, and fault zone head waves: Tectonophysics, v. 721, p. 56–69, https://doi.org/10.1016/j.tecto.2017.09.003.

Allen, J.R.L., 1978, Studies in fluviatile sedimentation: An exploratory quantitative model for the architecture of avulsion controlled alluvial sites: Sedimentary Geology, v. 21, p. 129–147, https://doi.org/10.1016/0037-0738(78)90002-7.

Amato, J.M., Pavlis, T.L., Clift, P.D., Kochelek, E.J., Hecker, J.P., Worthman, C.M., and Day, E.M., 2013, Architecture of the Chugach accretionary complex as revealed by detrital zircon ages and lithologic variations: Evidence for Mesozoic subduction erosion in south-central Alaska: Geological Society of America Bulletin, v. 125, p. 1891–1911, https://doi.org/10.1130/B30818.1.

Andronicos, C.L., Hollister, L.S., Davidson, C., and Chardon, D., 1999, Kinematics and tectonic significance of transpressive structures within the Coast Plutonic Complex, British Columbia: Journal of Structural Geology, v. 21, p. 229–243, https://doi.org/10.1016/S0191-8141(98)00117-5.

Arkle, J.C., Armstrong, P.A., Haeussler, P.J., Prior, M.G., Hartman, S., Sendziak, K.L., and Brush, J.A., 2013, Focused exhumation in the syntaxis of the western Chugach Mountains and Prince William Sound, Alaska: Geological Society of America Bulletin, v. 125, p. 776–793, https://doi.org/10.1130/B30738.1.

Bacon, C.R., Vazquez, J.A., and Wooden, J.L., 2012, Peninsular terrane basement ages recorded by Paleozoic and Paleoproterozoic zircon in gabbro xenoliths and andesite from Redoubt volcano, Alaska: Geological Society of America Bulletin, v. 124, p. 24–34 https://doi.org/10.1130/B30439.1.

Barker, F., Aleinikoff, J.N., Box, S., Evans, B.W., Gehrels, G., Hill, M.D., Irving, A.J., Kelley, J.S., Leeman, W.P., Lull, J.S., Nokleberg, W.J., Pallister, J.S., Patrick, B.E., Plafker, G., and Rubin, C.M., 1994, Some accreted volcanic rocks of Alaska and their elemental abundances, *in* Plafker, G., and Berg, H., eds., The Geology of Alaska: Boulder, Colorado, Geological Society of America, The Geology of North America, v. G-1, p. 555–588, https://doi.org/10.1130/DNAG-GNA-G1.555.

Batt, G.E., Baldwin, S.L., Cottam, M.A., Fitzgerald, P.G., Brandon, M.T., and Spell, T.L., 2004, Cenozoic plate boundary evolution in the South Island of New Zealand: New thermochronological constraints: Tectonics, v. 23, no. 4, TC4001, https://doi.org/10.1029/2003TC001527.

Benowitz, J.A., Layer, P.W., Armstrong, P.A., Perry, S.E., Haeussler, P.J., Fitzgerald, P.G., and VanLaningham, S., 2011, Spatial variations in focused exhumation along a continental-scale strike-slip fault: The Denali fault of the eastern Alaska Range: Geosphere, v. 7, p. 455–467, https://doi.org/10.1130/GES00589.1.

Benowitz, J.A., Haeussler, P.J., Layer, P.W., O'Sullivan, P., Wallace, W.K., and Gillis, R.J., 2012, Cenozoic tectono-thermal history of the Tordrillo Mountains, Alaska: Paleocene–Eocene ridge subduction, decreasing relief, and late Neogene faulting: Geochemistry Geophysics Geosystems, v. 13, Q04009, https://doi.org/10.1029/2011GC003951.

Benowitz, J.A., Layer, P.W., and Vanlaningham, S., 2014, Persistent long-term (c. 24 Ma) exhumation in the eastern Alaska Range constrained by stacked thermochronology, *in* Jourdan, F., Mark, D.F., and Verati, C., eds., Advances in $^{40}Ar/^{39}Ar$ Dating: From Archaeology to Planetary Sciences: Geological Society [London] Special Publication 378, p. 225–243, https://doi.org/10.1144/SP378.12.

Benowitz, J.A., Davis, K., and Roeske, S., 2019, A river runs through it both ways across time: $^{40}Ar/^{39}Ar$ detrital and bedrock muscovite geochronology constraints on the Neogene paleodrainage history of the Nenana River system, Alaska Range: Geosphere, v. 15, p. 682–701, https://doi.org/10.1130/GES01673.1.

Beranek, L.P., and Mortensen, J.K., 2011, The timing and provenance record of the Late Permian Klondike orogeny in northwestern Canada and arc-continent collision along western North America: Tectonics, v. 30, TC5017, https://doi.org/10.1029/2010TC002849.

Beranek, L.P., van Staal, C.R., McClelland, W.C., Israel, S., and Mihalynuk, M.G., 2013, Baltican crustal provenance for Cambrian–Ordovician sandstones of the Alexander terrane, North American Cordillera: Evidence from detrital zircon U-Pb geochronology and Hf isotope geochemistry: Journal of the Geological Society [London], v. 170, p. 7–18, https://doi.org/10.1144/jgs2012-028.

Beranek, L.P., van Staal, C.R., McClelland, W.C., Joyce, N., and Israel, S., 2014, Late Paleozoic assembly of the Alexander-Wrangellia-Peninsular composite terrane, Canadian and Alaskan Cordillera: Geological Society of America Bulletin, v. 126, p. 1531–1550, https://doi.org/10.1130/31066.1.

Berg, H.C., Jones, D.L., and Richter, D.H., 1972, Gravina-Nutzotin Belt: Tectonic Significance of an Upper Mesozoic Sedimentary

and Volcanic Sequence in Southern and Southeastern Alaska: U.S. Geological Survey Professional Paper 800D, p. D1–D24.
Betka, P.M., Gillis, R.J., and Benowitz, J.A., 2017, Cenozoic sinistral transpression and polyphase slip within the Bruin Bay fault system, Iniskin-Tuxedni region, Cook Inlet, Alaska: Geosphere, v. 13, p. 1806–1833, https://doi.org/10.1130/GES01464.1.
Bier, S., and Fisher, D., 2003, Structure and kinematics of a transect across the Kahiltna assemblage, south-central Alaska: Geological Society of America Abstracts with Programs, v. 35, no. 6, p. 560.
Bier, S., Fischer, D., Feineman, M., and O'Sullivan, P.B., 2017, Structural fabrics, geochemistry, and geochronology of the Reindeer Hills mélange, a suture zone in south-central Alaska: Geological Society of America Abstracts with Programs, v. 49, no. 6, paper 322-4, https://doi.org/10.1130/abs/2017AM-305230.
Bliss, B., Trop, J.M., and Benowitz, J.A., 2017, Paleozoic magmatism in the Wrangellia terrane constrained by U-Pb geochronology of modern river detrital zircons, Wrangell Mountains, Alaskan Cordillera: Geological Society of America Abstracts with Programs, v. 49, no. 6, paper 389-5, https://doi.org/10.1130/abs/2017AM-296860.
Braman, D.R., 2001, Terrestrial palynomorphs of the Upper Santonian?–Lower Campanian Milk River Formation, southern Alberta, Canada: Palynology, v. 25, p. 57–107.
Brennan, P.R., Gilbert, H., and Ridgway, K.D., 2011, Crustal structure across the central Alaska Range: Anatomy of a Mesozoic collisional zone: Geochemistry Geophysics Geosystems, v. 12, no. 4, Q04010, https://doi.org/10.1029/2011GC003519.
Bridge, J.S., and Lunt, I.A., 2006, Depositional models of braided rivers, *in* Sambrook-Smith, G.H., Best, J.L., Bristow, C.S., and Petts, G.E., eds., Braided Rivers: Process, Deposits, Ecology and Management: Oxford, UK, Blackwell Publishing, p. 11–50, https://doi.org/10.1002/9781444304374.ch2.
Brueseke, M.E., Benowitz, J.A., Trop, J.M., Davis, K.D., Berkelhammer, P.W., Layer, P.W., and Morter, B.K., 2019, The Alaska Wrangell arc: ~30 Ma of subduction-related magmatism along a still active arc-transform junction: Terra Nova, v. 31, p. 59–66, https://doi.org/10.1111/ter.12369.
Burden, E.T., 1984, Terrestrial palynomorph biostratigraphy of the lower part of the Mannville Group (Lower Cretaceous), Alberta and Montana, *in* Stott, D.F., and Glass, D.J., eds., The Mesozoic of Middle North America: Canadian Society of Petroleum Geologists Memoir 9, p. 249–269.
Burkett, C.A., Bemis, S.P., and Benowitz, J.A., 2016, Along-fault migration of the Mount McKinley restraining bend of the Denali fault defined by late Quaternary fault patterns and seismicity, Denali National Park and Preserve, Alaska: Tectonophysics, v. 693, p. 489–506, https://doi.org/10.1016/j.tecto.2016.05.009.
Butler, R.F., Gehrels, G.E., Hart, W., Davidson, C., and Crawford, M.L., 2006, Paleomagnetism of Late Jurassic to mid-Cretaceous plutons near Prince Rupert, British Columbia, *in* Haggart, J.W., Enkin, R.J., and Monger, J.W.H., eds., Paleogeography of the North American Cordillera: Evidence For and Against Large-Scale Displacements: Geological Association of Canada Special Paper 46, p. 171–200.
Cas, R.A.F., and Wright, J.V., 1987, Volcanic Successions, Modern and Ancient: A Geological Approach to Processes Products and Successions: London, UK, Chapman, 544 p.
Cavazza, W., Albino, I., Zattin, M., Galoyan, G., Imamverdiyev, N., and Melkonyan, R., 2017, Thermochronometric evidence for Miocene tectonic reactivation of the Sevan–Akera suture zone (Lesser Caucasus): A far-field tectonic effect of the Arabia–Eurasia collision?, *in* Sosson, M., Stephenson, R.A., and Adamia, S.A., eds., Tectonic Evolution of the Eastern Black Sea and Caucasus: Geological Society of London Special Publication 428, p. 187–198, https://doi.org/10.1144/SP428.4.
Cecil, M.R., Gehrels, G., Ducea, M.N., and Patchett, P.J., 2011, U-Pb-Hf characterization of the central Coast Mountains batholith: Implications for petrogenesis and crustal architecture: Lithosphere, v. 3, p. 247–260, https://doi.org/10.1130/L134.1.
Cecil, M.R., Rusmore, M.E., Gehrels, G.E., Woodsworth, G.J., Stowell, H.H., Yokelson, I.N., Chisom, C., Trautman, M., and Homan, E., 2018, Along-strike variation in the magmatic tempo of the Coast Mountains Batholith, British Columbia, and implications for processes controlling episodicity in arcs: Geochemistry Geophysics Geosystems, v. 19, p. 4274–4289, https://doi.org/10.1029/2018GC007874.
Chardon, D., 2003, Strain partitioning and batholith emplacement at the root of a transpressive magmatic arc: Journal of Structural Geology, v. 25, p. 91–107, https://doi.org/10.1016/S0191-8141(02)00015-9.
Chardon, D., Andronicos, C.L., and Hollister, L.S., 1999, Large-scale transpressive shear zone patterns and displacements within magmatic arcs: The Coast Plutonic Complex, British Columbia: Tectonics, v. 18, p. 278–292, https://doi.org/10.1029/1998TC900035.
Cobbett, R., Israel, S., Mortensen, J., Joyce, N., and Crowley, J., 2016, Structure and kinematic evolution of the Duke River fault, southwestern Yukon: Canadian Journal of Earth Sciences, v. 54, p. 322–344, https://doi.org/10.1139/cjes-2016-0074.
Cohen, H.A., and Lundberg, N., 1993, Detrital record of the Gravina arc, southeastern Alaska: Petrology and provenance of Seymour Canal Formation sandstones: Geological Society of America Bulletin, v. 105, p. 1400–1414, https://doi.org/10.1130/0016-7606(1993)105<1400:DROTGA>2.3.CO;2.
Cohen, H.A., Hall, C.M., and Lundberg, N., 1995, $^{40}Ar/^{39}Ar$ dating of detrital grains constrains the provenance and stratigraphy of the Seymour Canal Formation, Gravina belt, southeastern Alaska: The Journal of Geology, v. 103, p. 327–337, https://doi.org/10.1086/629750.
Collinson, J.D., 1996, Alluvial sediments, *in* Reading, H.G., ed., Sedimentary Environments: Processes, Facies, and Stratigraphy: Oxford, UK, Blackwell Science, p. 37–82.
Colpron, M., Nelson, J.L., and Murphy, D.C., 2007, Northern Cordilleran terranes and their interactions through time: GSA Today, v. 17, no. 4/5, p. 4–10, https://doi.org/10.1130/GSAT01704-5A.1.
Coney, P.J., Jones, D.L., and Monger, J.W., 1980, Cordilleran suspect terranes: Nature, v. 288, p. 329–333.
Cowan, D.S., Brandon, M.T., and Garver, J.I., 1997, Geologic test of hypotheses for large coastwise displacement—A critique illustrated by the Baja British Columbia hypothesis: American Journal of Science, v. 297, p. 117–173, https://doi.org/10.2475/ajs.297.2.117.
Crawford, M.L., Hollister, L.S., and Woodsworth, G.J., 1987, Crustal deformation and regional metamorphism across a terrane boundary, Coast plutonic complex, British Columbia: Tectonics, v. 6, p. 343–361, https://doi.org/10.1029/TC006i003p00343.
Csejtey, B., Jr., Mullen, M.W., Cox, D.P., and Stricker, G.D., 1992, Geology and geochronology of the Healy quadrangle, south-central Alaska, U.S. Geological Survey Miscellaneous Investigations Series Map 1961, 1:250,000 scale.
Davidson, C., Hollister, L.S., and Schmid, S.M., 1992, Role of melt in the formation of a deep-crustal compressive shear zone: The Maclaren Glacier metamorphic belt, south central Alaska: Tectonics, v. 11, p. 348–359, https://doi.org/10.1029/91TC02907.
Day, W.C., O'Neill, J.M., Dusel-Bacon, C., Aleinikoff, J.N., and Siron, C.R., 2014, Geologic Map of the Kechumstuk Fault Zone in the Mount Veta Area, Fortymile Mining District, East-Central Alaska: U.S. Geological Survey Investigation Series Map 3291, scale 1:63,360.
Dewey, J.F., 1977, Suture zone complexities: A review: Tectonophysics, v. 40, p. 53–67, https://doi.org/10.1016/0040-1951(77)90029-4.
Dodds, C.J., and Campbell, R.B., 1992, Overview, legend, and mineral deposit tabulations for geology of SW Kluane Lake (115G and G (E1/2)), Mount Saint Elias (115B and C (E1/2)), SW Dezadeash (115A), NE Yakutat (114O), and Tatshenshini (114P) map areas, Yukon Territory and British Columbia: Geological Survey of Canada, Open Files 2188, no. 2191.
Dusel-Bacon, C., and Williams, I.S., 2009, Evidence for prolonged mid-Paleozoic plutonism and ages of crustal sources in east-central Alaska from SHRIMP U-Pb dating of syn-magmatic, inherited, and detrital zircon: Canadian Journal of Earth Sciences, v. 46, p. 21–39.
Dusel-Bacon, C., Hopkins, M.J., Mortenson, J.K., Dashevsky, S.S., Bressler, J.R., and Day, W.C., 2006, Paleozoic tectonic and metallogenic evolution of the pericratonic rocks of east-central Alaska and adjacent Yukon Territory, *in* Colpron, M., and Nelson, J.L., eds., Paleozoic Evolution and Metallogeny of Pericratonic Terranes at the Ancient Pacific Margin of North America, Canadian and Alaskan Cordillera: Geological Association of Canada Special Paper 45, p. 25–74.
Duvall, A.R., Clark, M.K., van der Pluijm, B.A., and Li, C., 2011, Direct dating of Eocene reverse faulting in northeastern Tibet using Ar-dating of fault clays and low-temperature thermochronometry: Earth and Planetary Science Letters, v. 304, no. 3–4, p. 520–526, https://doi.org/10.1016/j.epsl.2011.02.028.
Eberhart-Phillips, D., Haeussler, P.J., Freymueller, J.T., Frankel, A.D., Rubin, C.M., Craw, P., Ratchkovski, N.A., Anderson, G., Carver, G.A., Crone, A.J., and Dawson, T.E., 2003, The 2002 Denali fault earthquake, Alaska: A large magnitude, slip-partitioned event: Science, v. 300, p. 1113–1118, https://doi.org/10.1126/science.1082703.
Eisbacher, G.H., 1976a, Sedimentology of the Dezadeash flysch and its implications for strike-slip faulting along the Denali fault, Yukon Territory and Alaska: Canadian Journal of Earth Sciences, v. 13, p. 1495–1513, https://doi.org/10.1139/e76-157.
Eisbacher, G.H., 1976b, The Dezadeash flysch, eastern St. Elias Mountains, Canada, and its relationship to the Gravina-Nutzotin belt, Alaska: A discussion, *in* Miller, T.P., ed., Recent and Ancient Sedimentary Environments in Alaska: Anchorage, Alaska, Alaska Geological Society, p. G1–G4.
Engebretson, D.C., Cox, A., and Gordon, R.G., 1985, Relative Motions Between Oceanic and Continental Plates in the Pacific Basin: Geological Society of America Special Paper 206, 60 p., https://doi.org/10.1130/SPE206-p1.
Enkelmann, E., Zeitler, P.K., Garver, J.I., Pavlis, T.L., and Hooks, B.P., 2010, The thermochronological record of tectonic and

surface process interaction at the Yakutat–North American collision zone in southeast Alaska: American Journal of Science, v. 310, p. 231–260, https://doi.org/10.2475/04.2010.01.

Evenchick, C.A., McMechan, M.E., McNicoll, V.J., and Carr, S.D., 2007, A synthesis of the Jurassic–Cretaceous tectonic evolution of the central and southeastern Canadian Cordillera: Exploring links across the orogen, *in* Sears, J.W., Harms, T.A., and Evenchick, C.A., eds., Whence the Mountains? Inquiries into the Evolution of Orogenic Systems: A Volume in Honor of Raymond A. Price: Geological Society of America Special Paper 433, p. 117–145, https://doi.org/10.1130/2007.2433(06).

Fasulo, C.F., Ridgway, K.D., Allen, W.K., Romero, M.C., and Keough, B., 2018, U-Pb and Hf isotope detrital zircon geochronology of the Nutzotin Mountains sequence, south-central Alaska: Implications for the configuration of the Mesozoic convergent margin, NW Cordillera: Geological Society of America Abstracts with Programs, v. 50, no. 6, paper 46-7, https://doi.org/10.1130/abs/2018AM-322455.

Finzel, E.S., Trop, J.M., Ridgway, K.D., and Enkelmann, E., 2011, Upper plate proxies for flat-slab subduction processes in southern Alaska: Earth and Planetary Science Letters, v. 303, p. 348–360, https://doi.org/10.1016/j.epsl.2011.01.014.

Fiorillo, A.R., 2006, Review of the dinosaur record of Alaska with comments regarding Korean dinosaurs as comparable high-latitude fossil faunas: Journal of the Paleontological Society of Korea, v. 22, p. 15–27.

Fiorillo, A.R., Adams, T.L., and Kobayashi, Y., 2012, New sedimentological, palaeobotanical, and dinosaur ichnological data on the palaeoecology of an unnamed Late Cretaceous rock unit in Wrangell–St. Elias National Park and Preserve, Alaska, USA: Cretaceous Research, v. 37, p. 291–299, https://doi.org/10.1016/j.cretres.2012.04.013.

Fitzgerald, P.G., Roeske, S.M., Benowitz, J.A., Riccio, S.J., Perry, S.E., and Armstrong, P.A., 2014, Alternating asymmetric topography of the Alaska Range along the strike-slip Denali fault: Strain partitioning and lithospheric control across a terrane suture zone: Tectonics, v. 33, p. 1519–1533, https://doi.org/10.1002/2013TC003432.

Foster, H.L., Keith, T.E.C., and Menzie, W.D., 1994, Geology of the Yukon-Tanana area of east-central Alaska, *in* Plafker, G., and Berg, H.C., eds., The Geology of Alaska: Boulder, Colorado, Geological Society of America, The Geology of North America, v. G-1, p. 205–240, https://doi.org/10.1130/DNAG-GNA-G1.205.

Gabrielse, H., Murphy, D.C., and Mortensen, J.K., 2006, Cretaceous and Cenozoic dextral orogen-parallel displacements, magmatism, and paleogeography, north central Canadian Cordillera, *in* Haggart, J.W., Enkin, R.J., and Monger, J.W.H., eds., Paleogeography of the North American Cordillera: Evidence For and Against Large-Scale Displacements: Geological Association of Canada Special Paper 46, p. 255–276.

Garver, J.I., and Davidson, C.M., 2015, Southwestern Laurentian zircons in Upper Cretaceous flysch of the Chugach–Prince William terrane in Alaska: American Journal of Science, v. 315, p. 537–556, https://doi.org/10.2475/06.2015.02.

Gehrels, G., Rusmore, M., Woodsworth, G., Crawford, M., Andronicos, C., Hollister, L., Patchett, J., Ducea, M., Butler, R., Klepeis, K., and Davidson, C., 2009, U-Th-Pb geochronology of the Coast Mountains Batholith in north-coastal British Columbia: Constraints on age, petrogenesis, and tectonic evolution: Geological Society of America Bulletin, v. 121, p. 1341–1361, https://doi.org/10.1130/B26404.1.

Gehrels, G.E., 2000, Reconnaissance geology and U-Pb geochronology of the western flank of the Coast Mountains between Juneau and Skagway, southeastern Alaska, *in* Stowell, H.H., and McClelland, W.C., eds., Tectonics of the Coast Mountains in SE Alaska and Coastal British Columbia: Geological Society of America Special Paper 343, p. 213–234.

Gehrels, G.E., 2012, Detrital zircon U-Pb geochronology: Current methods and new opportunities, *in* Busby, C., and Azor, A., eds., Tectonics of Sedimentary Basins: Recent Advances: Oxford, UK, Wiley-Blackwell Publishing, p. 45–62, https://doi.org/10.1002/9781444347166.ch2.

Gehrels, G.E., 2014, Detrital zircon U-Pb geochronology applied to tectonics: Annual Review of Earth and Planetary Sciences, v. 42, p. 127–149, https://doi.org/10.1146/annurev-earth-050212-124012.

Gehrels, G.E., McClelland, W.C., Samson, S.D., Patchett, P.J., and Orchard, M.J., 1992, Geology of the western flank of the Coast Mountains between Cape Fanshaw and Taku Inlet, southeastern Alaska: Tectonics, v. 11, p. 567–585, https://doi.org/10.1029/92TC00482.

Gehrels, G.E., Valencia, V.A., and Ruiz, J., 2008, Enhanced precision, accuracy, efficiency, and spatial resolution of U-Pb ages by laser ablation–multicollector–inductively coupled plasma–mass spectrometry: Geochemistry Geophysics Geosystems, v. 9, Q03017, https://doi.org/10.1029/2007GC001805.

Goldfarb, R.J., Anderson, E.D., and Hart, C.J., 2013, Tectonic setting of the Pebble and other copper-gold-molybdenum porphyry deposits within the evolving middle Cretaceous continental margin of northwestern North America: Economic Geology and the Bulletin of the Society of Economic Geologists, v. 108, p. 405–419, https://doi.org/10.2113/econgeo.108.3.405.

Graham, G.E., Kelley, K.D., Holm-Denoma, C.S., Ayuso, R.A., Kokaly, R.F., Hoefen, T.M., and Selby, D., 2016, Geochronology and Nd-Sr-Pb isotopic compositions of Early Cretaceous intrusions and associated porphyry Cu deposits in eastern Alaska, *in* 35th International Geological Congress, Cape Town, South Africa, 27 August–4 September 2016, Paper 4858.

Grantz, A., 1964, Stratigraphic Reconnaissance of the Matanuska Formation in the Matanuska Valley, Alaska: U.S. Geological Survey Bulletin 1181-I, 33 p.

Grantz, A., Jones, D.L., and Lanphere, M.A., 1966, Stratigraphy, Paleontology, and Isotopic Ages of Upper Mesozoic Rocks in the Southwestern Wrangell Mountains, Alaska: U.S. Geological Survey Professional Paper 550-C, p. 39–47.

Haeussler, P.J., Gehrels, G.E., and Karl, S.M., 2006, Constraints on the Age and Provenance of the Chugach Accretionary Complex from Detrital Zircons in the Sitka Graywacke near Sitka, Alaska: U.S. Geological Survey Professional Paper 1709F, 24 p.

Hampton, B.A., Ridgway, K.D., O'Neill, J.M., Gehrels, G.E., Schmidt, J., and Blodgette, R.B., 2007, Pre-, syn-, and post-depositional stratigraphic framework and provenance of Upper Triassicé–Upper Cretaceous strata in the northwestern Talkeetna Mountains, Alaska, *in* Ridgway, K.D., Trop, J.M., Glen, J.M.G., and O'Neill, J.M., eds., Tectonic Growth of a Collisional Continental Margin: Crustal Evolution of Southern Alaska: Geological Society of America Special Paper 431, p. 401–438, https://doi.org/10.1130/2007.2431(16).

Hampton, B.A., Ridgway, K.D., and Gehrels, G.E., 2010, A detrital record of Mesozoic island arc accretion and exhumation in the North American Cordillera: U-Pb geochronology of the Kahiltna basin, southern Alaska: Tectonics, v. 29, TC4015, https://doi.org/10.1029/2009TC002544.

Hampton, B.A., Jacobs, M.R., and Stopka, C.J., 2017, U-Pb detrital geochronology and Hf isotopic analyses from Upper Cretaceous strata of the northern Talkeetna Mountains, southern Alaska: Sediment dispersal and magmatism during the final accretionary phase of the Wrangellia composite terrane: Geological Society of America Abstracts with Programs, v. 49, no. 6, paper 344-14, https://doi.org/10.1130/abs/2017AM-308255.

Haq, B.U., 2014, Cretaceous eustasy revisited: Global and Planetary Change, v. 113, p. 44–58, https://doi.org/10.1016/j.gloplacha.2013.12.007.

Hendrix, M.S., Graham, S.A., Amory, J.Y., and Badarch, G., 1996, Noyon Uul syncline, southern Mongolia: Lower Mesozoic sedimentary record of the tectonic amalgamation of central Asia: Geological Society of America Bulletin, v. 108, p. 1256–1274, https://doi.org/10.1130/0016-7606(1996)108<1256:NUSSML>2.3.CO;2.

Herman, A.B., and Sokolova, A.B., 2016, Late Cretaceous Kholokhovchan flora of northeastern Asia: Composition, age and fossil plant descriptions: Cretaceous Research, v. 59, p. 249–271, https://doi.org/10.1016/j.cretres.2015.11.008.

Holdsworth, R.E., Handa, M., Miller, J.A., and Buick, I.S., 2001, Continental reactivation and reworking: An introduction, *in* Miller, J.A., Holdsworth, R.E., Buick, I.S., and Hand, M., eds., Continental Reactivation and Reworking: Geological Society of London Special Publication 184, p. 1–12, https://doi.org/10.1144/GSL.SP.2001.184.01.01.

Hollick, A., 1930, The Upper Cretaceous Floras of Alaska: U.S. Geological Survey Professional Paper 159, 123 p.

Hults, C.P., Wilson, F.H., Donelick, R.A., and O'Sullivan, P.B., 2013, Two flysch belts having distinctly different provenance suggest no stratigraphic link between the Wrangellia composite terrane and the paleo-Alaskan margin: Lithosphere, v. 5, p. 575–594, https://doi.org/10.1130/L310.1.

Johnson, C.L., and Graham, S.A., 2004, Cycles in perilacustrine facies of late Mesozoic rift basins, southeastern Mongolia: Journal of Sedimentary Research, v. 74, p. 786–804, https://doi.org/10.1306/051304740786.

Jones, D.L., Silberling, N.J., Gilbert, W., and Coney, P., 1982, Character, distribution, and tectonic significance of accretionary terranes in the central Alaska Range: Journal of Geophysical Research, v. 87, p. 3709–3717, https://doi.org/10.1029/JB087iB05p03709.

Kalbas, J.L., Ridgway, K.D., and Gehrels, G.E., 2007, Stratigraphy, depositional systems, and provenance of the Lower Cretaceous Kahiltna assemblage, western Alaska Range: Basin development in response to oblique collision, *in* Ridgway, K.D., Trop, J.M., Glen, J.M.G., and O'Neill, J.M., eds., Tectonic Growth of a Collisional Continental Margin: Crustal Evolution of Southern Alaska: Geological Society of America Special Paper 431, p. 307–343, https://doi.org/10.1130/2007.2431(13).

Kapp, P.A., and Gehrels, G.E., 1998, Detrital zircon constraints on the tectonic evolution of the Gravina belt, southeastern

Alaska: Canadian Journal of Earth Sciences, v. 35, p. 253–268, https://doi.org/10.1139/e97-110.

Laskowski, A.K., Kapp, P., Ding, L., Campbell, C., and Liu, X., 2017, Tectonic evolution of the Yarlung suture zone, Lopu Range region, southern Tibet: Tectonics, v. 36, p. 108–136, https://doi.org/10.1002/2016TC004334.

Layer, P.W., 2000, Argon-40/argon-39 age of the El'gygytgyn impact event, Chukotka, Russia: Meteoritics and Planetary Science, v. 35, p. 591–599, https://doi.org/10.1111/j.1945-5100.2000.tb01439.x.

Layer, P.W., Hall, C.M., and York, D., 1987, The derivation of $^{40}Ar/^{39}Ar$ age spectra of single grains of hornblende and biotite by laser step heating: Geophysical Research Letters, v. 14, p. 757–760, https://doi.org/10.1029/GL014i007p00757.

Leloup, P.H., Boutonnet, E., Davis, W.J., and Hattori, K., 2011, Long-lasting intracontinental strike-slip faulting: New evidence from the Karakorum shear zone in the Himalayas: Terra Nova, v. 23, p. 92–99.

Le Maitre, R.W., Streckeisen, A.L., Zanettin, B., Le Bas, M.J., Bonin, B., and Bateman, P., eds., 2002, Igneous Rocks: A Classification and Glossary of Terms: Cambridge, UK, Cambridge University Press, 236 p., https://doi.org/10.1017/CBO9780511535581.

LePage, B., 2009, Earliest occurrence of *Taiwania* (Cupressaceae) from the Early Cretaceous of Alaska: Evolution, biogeography, and paleoecology: Proceedings of the Academy of Natural Sciences of Philadelphia, v. 158, p. 129–158, https://doi.org/10.1635/053.158.0107.

Lovera, O.M., Grove, M., and Harrison, T.M., 2002, Systematic analysis of K-feldspar $^{40}Ar/^{39}Ar$ step heating results II: Relevance of laboratory argon diffusion properties to nature: Geochimica et Cosmochimica Acta, v. 66, p. 1237–1255, https://doi.org/10.1016/S0016-7037(01)00846-8.

Lowey, G.W., 1998, A new estimate of the amount of displacement on the Denali fault system based on the occurrence of carbonate megaboulders in the Dezadeash Formation (Jura–Cretaceous), Yukon, and the Nutzotin Mountains sequence (Jura–Cretaceous), Alaska: Bulletin of Canadian Petroleum Geology, v. 46, p. 379–386.

Lowey, G.W., 2007, Lithofacies analysis of the Dezadeash Formation (Jura–Cretaceous), Yukon, Canada: The depositional architecture of a mud/sand-rich turbidite system: Sedimentary Geology, v. 198, p. 273–291, https://doi.org/10.1016/j.sedgeo.2006.12.011.

Lowey, G.W., 2011, Volcaniclastic gravity flow deposits in the Dezadeash Formation (Jura-Cretaceous), Yukon, Canada: Implications regarding the tectonomagmatic evolution of the Chitina arc in the northern Cordillera of North America: Lithos, v. 125, p. 86–100, https://doi.org/10.1016/j.lithos.2011.01.014.

Lowey, G.W., 2018, Provenance analysis of the Dezadeash Formation (Jura-Cretaceous), Yukon, Canada: Implications regarding a linkage between the Wrangellia composite terrane and the western margin of Laurasia: Canadian Journal of Earth Sciences, v. 56, no. 1, p. 77–100, https://doi.org/10.1139/cjes-2017-0244.

Ludwig, K.R., 2008, Manual for Isoplot 3.7: Berkeley Geochronology Center, Special Publication 4, 77 p.

MacKevett, E.M., Jr., 1978, Geologic Map of the McCarthy Quadrangle, Alaska: U.S. Geological Survey Miscellaneous Investigation Series I-1032, scale 1:250,000.

Mahoney, J.B., Gordee, S.M., Haggart, J.W., Friedman, R.M., Diakow, L.J., and Woodsworth, G.J., 2009, Magmatic evolution of the eastern Coast Plutonic Complex, Bella Coola region, west-central British Columbia: Geological Society of America Bulletin, v. 121, p. 1362–1380, https://doi.org/10.1130/B26325.1.

Makaske, B., 2001, Anastomosing rivers: A review of their classification, origin and sedimentary products: Earth-Science Reviews, v. 53, p. 149–196, https://doi.org/10.1016/S0012-8252(00)00038-6.

Manselle, P., Brueseke, M.E., Trop, J.M., Benowitz, J.A., Snyder, D.C., and Hart, W.K., 2018, Mid-Cretaceous volcanism and fluvial-deltaic sedimentation associated with accretion of the Wrangellia composite terrane, Chisana arc, Gravina-Nutzotin belt, Alaska: Geological Society of America Abstracts with Programs, v. 50, no. 6, paper 49-1, https://doi.org/10.1130/abs/2018AM-319222.

Manuszak, J.D., 2000, Sedimentary and structural record of Late Jurassic–Early Cretaceous collisional tectonics, Nutzotin and Mentasta Mountains, east-central Alaska [Master's thesis]: Purdue University, 291 p.

Manuszak, J.D., Ridgway, K.D., Trop, J.M., and Gehrels, G.E., 2007, Sedimentary record of the tectonic growth of a collisional continental margin: Upper Jurassic–Lower Cretaceous Nutzotin Mountains sequence, eastern Alaska Range, Alaska, *in* Ridgway, K.D., Trop, J.M., Glen, J.M.G., and O'Neill, J.M., eds., Tectonic Growth of a Collisional Continental Margin: Crustal Evolution of Southern Alaska: Geological Society of America Special Paper 431, p. 345–377, https://doi.org/10.1130/2007.2431(14).

May, F.E., 1972, A survey of palynomorphs from several coal-bearing horizons of Utah, *in* Doelling, H.H., ed., Central Utah Coal Fields: Sevier-Sanpete, Wasatch Plateau, Book Cliffs and Emery: Utah Geological and Mineralogical Survey Monograph 3, p. 497–542.

May, F.E., and Traverse, A., 1973, Palynology of the Dakota Sandstone (Middle Cretaceous) near Bryce Canyon National Park, southern Utah: Geoscience and Man, v. 7, p. 57–64, https://doi.org/10.1080/00721395.1973.9989733.

McCabe, P.J., 1984, Depositional environments of coal and coal-bearing strata, *in* Rahmani, R.A., and Flores, R.M., Sedimentology of Coal and Coal-Bearing Sequences: Special Publication of the International Association of Sedimentologists, v. 7, p. 13–42, https://doi.org/10.1002/9781444303797.ch2.

McCabe, P.J., 1991, Geology of coal; environments of coal deposition, *in* Gluskoter, H.J., Rice, D.D., and Taylor, R.B., eds., Economic Geology, U.S.: Boulder, Colorado, Geological Society of America, The Geology of North America, v. P-2, p. 469–482.

McClelland, W.C., and Gehrels, G.E., 1990, The Duncan Canal shear zone: A right lateral shear zone of Jurassic age along the inboard margin of the Alexander terrane: Geological Society of America Bulletin, v. 102, p. 1378–1392, https://doi.org/10.1130/0016-7606(1990)102<1378:GOTDCS>2.3.CO;2.

McClelland, W.C., and Mattinson, J.M., 2000, Cretaceous–Tertiary evolution of the western Coast Mountains, central southeastern Alaska, *in* Stowell, H.H., and McClelland, W.C., eds., Tectonic Evolution of the Coast Mountains Orogen, Southeastern Alaska and Coastal British Columbia: Geological Society of American Special Paper 343, p. 159–182, https://doi.org/10.1130/0-8137-2343-4.159.

McClelland, W.C., Gehrels, G.E., and Saleeby, J.B., 1992, Upper Jurassic–Lower Cretaceous basinal strata along the Cordilleran margin: Implications for the accretionary history of the Alexander-Wrangellia-Peninsular terrane: Tectonics, v. 11, p. 823–835, https://doi.org/10.1029/92TC00241.

McDougall, I., and Harrison, T.M., 1999, Geochronology and Thermochronology by the $^{40}Ar/^{39}Ar$ Method (2nd ed.): New York, Oxford University Press, 269 p.

Melchor, R.N., 2007, Changing lake dynamics and sequence stratigraphy of synrift strata in a half-graben: An example from the Triassic Ischigualasto-Villa Union Basin, Argentina: Sedimentology, v. 54, p. 1,417–1,446, https://doi.org/10.1111/j.1365-3091.2007.00887.x.

Milde, E.R., 2014, Using Low-Temperature Thermochronology to Constrain the Role of the Totschunda Fault in Southeastern Alaskan Tectonics [Ph.D. dissertation]: Syracuse, New York, Syracuse University, 127 p.

Miall, A.D., 1978, Lithofacies types and vertical profile models in braided river deposits: A summary, *in* Miall, A.D., ed., Fluvial Sedimentology: Canadian Society of Petroleum Geologists Memoirs, v. 5, p. 597–604.

Miall, A.D., 2006, The Geology of Fluvial Deposits: Berlin, Springer, 582 p.

Moll-Stalcup, E.J., 1994, Latest Cretaceous and Cenozoic magmatism in mainland Alaska, *in* Plafker, G., and Berg, H.C., eds., The Geology of Alaska: Boulder, Colorado, Geological Society of America, The Geology of North America, v. G-1, p. 589–619.

Monger, J.W.H., 2014, Logan Medallist 1. Seeking the suture: The Coast-Cascade conundrum: Geoscience Canada, v. 41, p. 379–20, https://doi.org/10.12789/geocanj.2014.41.058.

Monger, J.W.H., van der Heyden, P., Journeay, J.M., Evenchick, C.A., and Mahoney, J.B., 1994, Jurassic–Cretaceous basins along the Canadian Coast belt: Their bearing on pre–mid-Cretaceous sinistral displacements: Geology, v. 22, p. 175–178, https://doi.org/10.1130/0091-7613(1994)022<0175:JCBATC>2.3.CO;2.

Najman, Y., Appel, E., Boudagher-Fadel, M., Brown, P., Carter, A., Garzanti, E., Godin, L., Han, J., Oliver, G., Parrish, R., and Vezzoli, G., 2010, Timing of the India-Asia collision: Geological, biostratigraphic, and paleomagnetic constraints: Journal of Geophysical Research, v. 115, B12416, https://doi.org/10.1029/2010JB007673.

Nelson, J., and Gehrels, G.E., 2007, Detrital zircon geochronology and provenance of the southeastern Yukon-Tanana terrane: Canadian Journal of Earth Sciences, v. 44, p. 297–316, https://doi.org/10.1139/e06-105.

Nokleberg, W.J., Aleinikoff, J.N., Lange, I.M., Silva, S.R., Miyaoka, R.T., Schwab, C.E., Zehner, R.E., Bond, G.C., Richter, D.H., Smith, T.E., and Stout, J.H., 1992, Preliminary geologic map of the Mount Hayes Quadrangle, eastern Alaska Range, Alaska: U.S. Geological Survey Open-File Report 92-594, 1:250,000 scale.

Orme, D.A., Carrapa, B., and Kapp, P., 2015, Sedimentology, provenance and geochronology of the Upper Cretaceous–Lower Eocene western Xigaze forearc basin, southern Tibet: Basin Research, v. 27, p. 387–411, https://doi.org/10.1111/bre.12080.

Pavlis, T.L., Amato, J.A., Trop, J.M., Ridgway, K.D., Roeske, S.M., and Gehrels, G.E., 2019, Subduction polarity in ancient arcs: A call to integrate geology and geophysics to decipher the Mesozoic tectonic history of the Northern Cordillera of North

America: GSA Today, v. 29, no. 11, https://doi.org/10.1130/GSATG402.1.

Payenberg, T.H.D., Braman, D.R., Davis, D.W., and Miall, A.D., 2002, Litho- and chronostratigraphic relationships of the Santonian–Campanian Milk River Formation in southern Alberta and Eagle Formation in Montana utilizing stratigraphy, U-Pb geochronology, and palynology: Canadian Journal of Earth Sciences, v. 39, p. 1553–1577, https://doi.org/10.1139/e02-050.

Pecha, M.E., Gehrels, G.E., McClelland, W.C., Giesler, D., White, C., and Yokelson, I., 2016, Detrital zircon U-Pb geochronology and Hf isotope geochemistry of the Yukon-Tanana terrane, Coast Mountains, southeast Alaska: Geosphere, v. 12, p. 1556–1574, https://doi.org/10.1130/GES01303.1.

Pierson, T.C., and Scott, K.M., 1985, Downstream dilution of a lahar: Transition from debris flow to hyperconcentrated streamflow: Water Resources Research, v. 21, p. 1,511–1,524, https://doi.org/10.1029/WR021i010p01511.

Plafker, G., and Berg, H.C., 1994, Overview of the geology and tectonic evolution of Alaska, *in* Plafker, G., and Berg, H.C., eds., The Geology of Alaska: Boulder, Colorado, Geological Society of America, The Geology of North America, v. G-1, p. 989–1021.

Plafker, G., Hudson, T., and Richter, D.H., 1977, Preliminary observations on late Cenozoic displacements along the Totschunda and Denali fault systems, *in* Blean, K.M., ed., The United States Geological Survey in Alaska; Accomplishments during 1976: U.S. Geological Survey Circular 751B, p. B67–B69.

Plafker, G., Nokleberg, W.J., and Lull, J.S., 1989, Bedrock geology and tectonic evolution of the Wrangellia, Peninsular, and Chugach terranes along the Trans-Alaska Crustal Transect in the Chugach Mountains and southern Copper River basin, Alaska: Journal of Geophysical Research, v. 94, p. 4255–4295, https://doi.org/10.1029/JB094iB04p04255.

Plafker, G., Moore, J.C., and Winkler, G.R., 1994, Geology of the southern Alaska margin, *in* Plafker, G., and Berg, H.C., eds., The Geology of Alaska: Boulder, Colorado, Geological Society of America, The Geology of North America, v. G-1 p. 389–450.

Pocock, S.A.J., 1978, Lowermost Jurassic spore-pollen assemblage from the Canadian Arctic: The Palaeobotanist, v. 25, p. 363–375.

Raymo, M.E., Ruddiman, W.F., and Froelich, P.N., 1988, Influence of late Cenozoic mountain building on ocean geochemical cycles: Geology, v. 16, p. 649–653, https://doi.org/10.1130/0091-7613(1988)016<0649:IOLCMB>2.3.CO;2.

Reid, M., Finzel, E.S., Enkelmann, E., and McClelland, W.C., 2018, Detrital zircon provenance of Upper Jurassic–Upper Cretaceous forearc basin strata on the Insular terranes, south-central Alaska, *in* Ingersoll, R.V., Lawton, T.F., and Graham, S.A., eds., Tectonics, Sedimentary Basins, and Provenance: A Celebration of William R. Dickinson's Career: Geological Society of America Special Paper 540, p. 1–20.

Renne, P.R., Deino, A.L., Walter, R.C., Turrin, B.D., Swisher, C.C., Becker, T.A., Curtis, G.H., Sharp, W.D., and Jaouni, A.R., 1994, Intercalibration of astronomical and radioisotopic time: Geology, v. 22, p. 783–786, https://doi.org/10.1130/0091-7613(1994)022<0783:IOAART>2.3.CO;2.

Renne, P.R., Mundil, R., Balco, G., Min, K., and Ludwig, K.R., 2010, Joint determination of ^{40}K decay constants and $^{40}Ar^*/^{40}K$ for the Fish Canyon sanidine standard, and improved accuracy for $^{40}Ar/^{39}Ar$ geochronology: Geochimica et Cosmochimica Acta, v. 74, p. 5349, https://doi.org/10.1016/j.gca.2010.06.017.

Riccio, S.J., Fitzgerald, P.G., Benowitz, J.A., and Roeske, S.M., 2014, The role of thrust faulting in the formation of the eastern Alaska Range: Thermochronological constraints from the Susitna Glacier thrust fault region of the intracontinental strike-slip Denali fault system: Tectonics, v. 33, p. 2195–2217, https://doi.org/10.1002/2014TC003646.

Richter, D.H., 1971, Reconnaissance Geologic Map and Section of the Nabesna A3 Quadrangle, Alaska: U.S. Geological Survey Miscellaneous Geologic Investigations Map I-655, scale 1:63,360.

Richter, D.H., 1976, Geologic Map of the Nabesna Quadrangle: U.S. Geological Survey Miscellaneous Geologic Investigations Map I-932, scale 1:250,000.

Richter, D.H., and Jones, D.L., 1973, Geologic Map of the Nabesna A2 Quadrangle: U.S. Geological Survey Miscellaneous Geologic Investigations Map I-749, scale 1:63,360.

Richter, D.H., and Matson, N.A., 1971, Quaternary faulting in the eastern Alaska Range: Geological Society of America Bulletin, v. 82, p. 1529–1540, https://doi.org/10.1130/0016-7606(1971)82[1529:QFITEA]2.0.CO;2.

Richter, D.H., Lanphere, M.A., and Matson, N.A., Jr., 1975, Granitic plutonism and metamorphism, eastern Alaska Range, Alaska: Geological Society of America Bulletin, v. 86, p. 819–829, https://doi.org/10.1130/0016-7606(1975)86<819:GPAMEA>2.0.CO;2.

Richter, D.H., Preller, C.C., Labay, K.A., and Shew, N.B., 2006, Geologic Map of the Wrangell–Saint Elias Park and Preserve, Alaska: U.S. Geological Survey Scientific Investigations Map 2877, scale 1:350,000.

Ridgway, K.D., and DeCelles, P.G., 1993, Stream-dominated alluvial-fan and lacustrine depositional systems in Cenozoic strike-slip basins, Denali fault system, Yukon Territory: Sedimentology, v. 40, p. 645–666, https://doi.org/10.1111/j.1365-3091.1993.tb01354.x.

Ridgway, K.D., Trop, J.M., Nokleberg, W.J., Davidson, C.M., and Eastham, K.R., 2002, Mesozoic and Cenozoic tectonics of the eastern and central Alaska Range: Progressive basin development and deformation in a suture zone: Geological Society of America Bulletin, v. 114, p. 1480–1504, https://doi.org/10.1130/0016-7606(2002)114<1480:MACTOT>2.0.CO;2.

Rioux, M., Hacker, B., Mattinson, J., Kelemen, P., Blusztajn, J., and Gehrels, G., 2007, Magmatic development of an intra-oceanic arc: High-precision U-Pb zircon and whole-rock isotopic analyses from the accreted Talkeetna arc, south-central Alaska: Geological Society of America Bulletin, v. 119, p. 1168–1184, https://doi.org/10.1130/B25964.1.

Roeske, S.M., Snee, L.W., and Pavlis, T.L., 2003, Dextral slip reactivation of an arc-forearc boundary during Late Cretaceous–early Eocene oblique convergence in the northern Cordillera, *in* Sisson, V.B., et al., eds., Geology of a Transpressional Orogen Developed during Ridge-Trench Interaction along the North Pacific Margin: Geological Society of America Special Paper 371, p. 141–169, https://doi.org/10.1130/0-8137-2371-X.141.

Rubin, C.M., and Saleeby, J.B., 1991, The Gravina sequence: Remnants of a mid-Mesozoic oceanic arc in southern southeast Alaska: Journal of Geophysical Research, v. 96, p. 14,551–14,568, https://doi.org/10.1029/91JB00591.

Rubin, C.M., and Saleeby, J.B., 1992, Tectonic history of the eastern edge of the Alexander terrane, southeast Alaska: Tectonics, v. 11, p. 586–602, https://doi.org/10.1029/91TC02182.

Rubin, C.M., Saleeby, J.B., Cowan, D.S., Brandon, M.T., and McGroder, M.F., 1990, Regionally extensive mid-Cretaceous west-vergent thrust system in the northwestern Cordillera: Implications for continental-margin tectonism: Geology, v. 18, p. 276–280, https://doi.org/10.1130/0091-7613(1990)018<0276:REMCWV>2.3.CO;2.

Rusmore, M.E., and Woodsworth, G.J., 1991, Coast Plutonic Complex: A mid-Cretaceous contractional orogeny: Geology, v. 19, p. 941–944, https://doi.org/10.1130/0091-7613(1991)019<0941:CPCAMC>2.3.CO;2.

Rusmore, M.E., and Woodsworth, G.J., 1994, Evolution of the eastern Waddington thrust belt and its relation to the mid-Cretaceous Coast Mountains arc, western: British Columbia: Tectonics, v. 13, p. 1052–1067, https://doi.org/10.1029/94TC01316.

Samson, S.D., and Alexander, E.C., 1987, Calibration of the interlaboratory $^{40}Ar/^{39}Ar$ dating standard, MMhb1: Chemical Geology, v. 66, p. 27–34.

Sandy, M.R., and Blodgett, R.B., 1996, Peregrinella (Brachiopoda; Rynchonellida) from the Early Cretaceous, Wrangellia terrane: Proceedings of the International Brachiopod Congress, v. 3, p. 239–242.

Short, E., Snyder, D.C., Trop, J.M., Hart, W.K., and Layer, P.W., 2005, New findings on Early Cretaceous volcanism within the allochthonous Wrangellia terrane, south-central Alaska: Stratigraphic, geochronologic, and geochemical data from the Chisana Formation, Nutzotin Mountains: Geological Society of America Abstracts with Programs, v. 37, no. 7, p. 81.

Sigloch, K., and Mihalynuk, M.G., 2013, Intra-oceanic subduction shaped the assembly of Cordilleran North America: Nature, v. 496, p. 50, https://doi.org/10.1038/nature12019.

Sigloch, K., and Mihalynuk, M.G., 2017, Mantle and geological evidence for a Late Jurassic–Cretaceous suture spanning North America: Geological Society of America Bulletin, v. 129, p. 1489–1520.

Singh, C., 1971, Lower Cretaceous Microfloras of the Peace River Area, Northwestern Alberta: Research Council of Alberta Bulletin 28, 299 p.

Slingerland, R., and Smith, N.D., 2004, River avulsions and their deposits: Annual Review of Earth and Planetary Sciences, v. 32, p. 257–285, https://doi.org/10.1146/annurev.earth.32.101802.120201.

Smith, G.A., 1986, Coarse-grained nonmarine volcaniclastic sediment: Terminology and depositional processes: Geological Society of America Bulletin, v. 97, p. 1–10, https://doi.org/10.1130/0016-7606(1986)97<1:CNVSTA>2.0.CO;2.

Snyder, D.E., and Hart, W.K., 2007, The White Mountain granitoid suite: Isotopic constraints on source reservoirs for Cretaceous magmatism within the Wrangellia terrane, *in* Ridgway, K.D., Trop, J.M., Glen, J.M.G., and O'Neill, J.M., eds., Tectonic Growth of a Collisional Continental Margin: Crustal Evolution of Southern Alaska: Geological Society of America Special Paper 431, p. 379–399, https://doi.org/10.1130/2007.2431(15).

Spicer, R.A., and Herman, A.B., 2002, The Albian–Cenomanian flora of the Kukpowruk River, western North Slope, Alaska: Stratigraphy, palaeofloristics, and plant communities: Cretaceous Research, v. 22, p. 1–40, https://doi.org/10.1006/cres.2000.0238.

Spicer, R.A., Ahlberg, A., Herman, A.B., Kelley, S.P., Raikevich, M.I., and Rees, P.M., 2002, Palaeoenvironment and ecology of

the middle Cretaceous Grebenka flora of northeastern Asia: Palaeogeography, Palaeoclimatology, Palaeoecology, v. 184, p. 65–105, https://doi.org/10.1016/S0031-0182(02)00247-X.

Spotila, J.A., Niemi, N., Brady, R., House, M., Buscher, J., and Oskin, M., 2007, Long-term continental deformation associated with transpressive plate motion: The San Andreas fault: Geology, v. 35, p. 967–970, https://doi.org/10.1130/G23816A.1.

Stamatakos, J.A., Trop, J.M., and Ridgway, K.D., 2001, Late Cretaceous paleogeography of Wrangellia: Paleomagnetism of the MacColl Ridge Formation, southern Alaska, revisited: Geology, v. 29, p. 947–950, https://doi.org/10.1130/0091-7613(2001)029<0947:LCPOWP>2.0.CO;2.

Stevens Goddard, A.L., Trop, J.M., and Ridgway, K.D., 2018, Detrital zircon record of a Mesozoic collisional forearc basin in south central Alaska: The tectonic transition from an oceanic to continental arc: Tectonics, v. 37, p. 529–557, https://doi.org/10.1002/2017TC004825.

Tochilin, C., Gehrels, G., Nelson, J., and Mahoney, J.B., 2014, U-Pb and Hf isotope analysis of detrital zircons from the Banks Island assemblage (coastal British Columbia) and southern Alexander terrane (southeast Alaska): Lithosphere, v. 6, p. 200–215, https://doi.org/10.1130/L338.1.

Trop, J.M., 2008, Latest Cretaceous forearc basin development along an accretionary convergent margin, south central Alaska: Geological Society of America Bulletin, v. 120, p. 207–224, https://doi.org/10.1130/B26215.1.

Trop, J.M., and Ridgway, K.D., 2007, Mesozoic and Cenozoic tectonic growth of southern Alaska: A sedimentary basin perspective, *in* Ridgway, K.D., Trop, J.M., Glen, J.M.G., and O'Neill, J.M., eds., Tectonic Growth of a Collisional Continental Margin: Crustal Evolution of Southern Alaska: Geological Society of America Special Paper 431, p. 55–94, https://doi.org/10.1130/2007.2431(04).

Trop, J.M., Ridgway, K.D., Manuszak, J.D., and Layer, P.W., 2002, Mesozoic sedimentary basin development on the allochthonous Wrangellia composite terrane, Wrangell Mountains basin, Alaska: A long-term record of terrane migration and arc construction: Geological Society of America Bulletin, v. 114, p. 693–717, https://doi.org/10.1130/0016-7606(2002)114<0693:MSBDOT>2.0.CO;2.

Trop, J.M., Szuch, D.A., Rioux, M., and Blodgett, R.B., 2005, Sedimentology and provenance of the Upper Jurassic Naknek Formation, Talkeetna Mountains, Alaska: Bearings on the accretionary tectonic history of the Wrangellia composite terrane: Geological Society of America Bulletin, v. 117, p. 570–588, https://doi.org/10.1130/B25575.1.

Trop, J.M., Snyder, D., Hart, W.K., and Idleman, B.D., 2012, Miocene basin development and volcanism along a strike-slip to flat-slab subduction transition: Stratigraphy, geochemistry, and geochronology of the central Wrangell volcanic belt, Yakutat–North America collision zone: Geosphere, v. 8, p. 805–834, https://doi.org/10.1130/GES00762.1.

Trop, J.M., Benowitz, J.A., Cole, R., and O'Sullivan, P., 2019, Cretaceous to Miocene magmatism, sedimentation, and exhumation within the Alaska Range suture zone: A reactivated terrane boundary: Geosphere, v. 15, p. 1066–1101, https://doi.org/10.1130/GES02014.1.

van der Heyden, P., 1992, A Middle Jurassic to Early Tertiary Andean-Sierran arc model for the Coast belt of British Columbia: Tectonics, v. 11, p. 82–97, https://doi.org/10.1029/91TC02183.

van der Plas, L., and Tobi, A.C., 1965, A chart for judging the reliability of point counting results: American Journal of Science, v. 263, p. 87–90, https://doi.org/10.2475/ajs.263.1.87.

Waldien, T.S., Roeske, S.M., Benowitz, J.A., Allen, W.K., Ridgway, K.D., and O'Sullivan, P.B., 2018, Late Miocene to Quaternary evolution of the McCallum Creek thrust system, Alaska: Insights for range-boundary thrusts in transpressional orogens: Geosphere, v. 14, p. 2379–2406, https://doi.org/10.1130/GES01676.1.

Walker, J.D., Geissman, J.W., Bowring, S.A., and Babcock, L.E., compilers, 2018, Geologic Time Scale v. 5.0: Geological Society of America, https://doi.org/10.1130/2018.CTS005R3C.

White, C., Gehrels, G., Pecha, M., Giesler, D., Yokelson, I., McClelland, W., and Butler, R., 2016, U-Pb and Hf isotope analysis of detrital zircons from Paleozoic strata of the southern Alexander terrane (southeast Alaska): Lithosphere, v. 8, p. 83–96, https://doi.org/10.1130/L475.1.

Wilson, F.H., Hults, C.P., Mull, C.G., and Karl, S.M., 2015, Geologic Map of Alaska: U.S. Geological Survey Scientific Investigations Map 3340, scale 1:1,584,000, https://doi.org/10.3133/sim3340.

Wingate, F.H., 1980, Plant microfossils from the Denton Shale Member of the Bokchito Formation (Lower Cretaceous, Albian) in southern Oklahoma: Oklahoma Geological Survey Bulletin, v. 130, p. 1–93.

Worthington, L.L., Van Avendonk, H.J.A., Gulick, S.P.S., Christeson, G.L., and Pavlis, T.L., 2012, Crustal structure of the Yakutat terrane and the evolution of subduction and collision in southern Alaska: Journal of Geophysical Research, v. 117, B01102, https://doi.org/10.1029/2011JB008493.

Wyld, S.J., Umhoefer, P.J., and Wright, J.E., 2006, Reconstructing northern Cordilleran terranes along known Cretaceous and Cenozoic strike-slip faults: Implications for the Baja British Columbia hypothesis and other models, *in* Haggart, J.W., Enkin, R.J., and Monger, J.W.H., eds., Paleogeography of the North American Cordillera: Evidence For and Against Large-Scale Displacements: Geological Association of Canada Special Paper 46, p. 277–298.

Yokelson, I., Gehrels, G.E., Pecha, M., Giesler, D., White, C., and McClelland, W.C., 2015, U-Pb and Hf isotope analysis of detrital zircons from Mesozoic strata of the Gravina belt, southeast Alaska: Tectonics, v. 34, p. 2052–2066, https://doi.org/10.1002/2015TC003955.

York, D., Hall, C.M., Yanase, Y., Hanes, J.A., and Kenyon, W.J., 1981, $^{40}Ar/^{39}Ar$ dating of terrestrial minerals with a continuous laser: Geophysical Research Letters, v. 8, p. 1136–1138, https://doi.org/10.1029/GL008i011p01136.

Zhu, B., Kidd, W.S., Rowley, D.B., Currie, B.S., and Shafique, N., 2005, Age of initiation of the India-Asia collision in the east-central Himalaya: The Journal of Geology, v. 113, p. 265–285, https://doi.org/10.1086/428805.